RSC Publishing Journal of Materials Chemistry

Rhenium solubility in borosilicate nuclear waste glass: implications for the processing and immobilization of technetium-99

Journal:	*Journal of Materials Chemistry*
Manuscript ID:	JM-ART-06-2012-033541
Article Type:	Paper
Date Submitted by the Author:	02-Jun-2012

Complete List of Authors:	Goel, Ashutosh; Pacific Northwest National Laboratory, Riley, Brian; Pacific Northwest National Laboratory, Liezers, Martin; Pacific Northwest National Laboratory, Schweiger, Michael; Pacific Northwest National Laboratory, Rodriguez, Carmen; Pacific Northwest National Laboratory, Windisch, Charles; Pacific Northwest National Laboratory, Fundamental and Computational Sciences Hrma, Pavel; Pacific Northwest National Laboratory, Kim, Dong-Sang; Pacific Northwest National Laboratory, McCloy, John; Pacific Northwest National Laboratory, Glass and Materials Science Lukens, Wayne; Lawrence Berkeley National Laboratory, Chemical Sciences Division Kruger, Albert; U.S. Department of Energy, Waste Treatment and Immobilization Plant Project Office Engineering Division

June 1, 2012

Ram Seshadri, Editor
Journal of Materials Chemistry
University of California
Santa Barbara, CA, USA

Dear Dr. Seshadri:

Please see the attached file for an original manuscript for exclusive submission to *Journal of Materials Chemistry* in the subject area of solid state materials. This work was performed primarily at the Pacific Northwest National Laboratory in Richland, WA.

"***Rhenium solubility in borosilicate nuclear waste glass: implications for the processing and immobilization of technetium-99***"
by A. Goel, B. J. Riley, M. Liezers, M. J. Schweiger, C. P. Rodriguez, C. F. Windisch, Jr., P. Hrma, D-S Kim, J. S. McCloy (corresponding author), W. Lukens, and A. A. Kruger.

In our work, we have determined for the first time the solubility of Re(VII) in sodium borosilicate glass, and found that it is much higher than assumed. We describe the novel method for performing these solubility tests, the crystalline forms produced above solubility, and the application of this information to processing of radioactive nuclear waste containing technetium-99.

We have included some extensive supplementary information to support our conclusions, but have retained the core of the story in the main manuscript.

We feel that this work will be of interest to the *Journal of Materials Chemistry* readership. Please feel free to contact me if you need additional information.

Sincerely,

John S. McCloy, Ph.D.
Team Lead, Glass and Materials Science
Radiological Materials and Technology Development Group
Energy & Environment Directorate

Pacific Northwest National Laboratory
902 Battelle Boulevard
P.O. Box 999, MSIN K6-24
Richland, WA 99352 USA
Tel: 509-372-4964

john.mccloy@pnl.gov
www.pnl.gov

Rhenium solubility in borosilicate nuclear waste glass: implications for the processing and immobilization of technetium-99

Ashutosh Goel, Brian J. Riley, Martin Liezers, Michael J. Schweiger, Carmen P. Rodriguez, Charles F. Windisch, Jr., Pavel Hrma, Dong-Sang Kim, John S. McCloy*

Pacific Northwest National Laboratory, Richland, WA 99352, USA

Wayne W. Lukens, Jr.

Lawrence Berkeley National Laboratory, Berkeley, CA 94720, USA

Albert A. Kruger

DOE-WTP Project Office Engineering Division, Richland, WA 99352, USA

Abstract

The immobilization of ^{99}Tc in a suitable host matrix has proved a challenging task for researchers in the nuclear waste community around the world. At the Hanford site in Washington State in the U.S., the total amount of ^{99}Tc in low-activity waste (LAW) is ~1,300 kg and the current strategy is to immobilize the ^{99}Tc in borosilicate glass with vitrification. In this context, the present article reports on the solubility and retention of rhenium, a nonradioactive surrogate for ^{99}Tc, in a LAW sodium borosilicate glass. Due to the radioactive nature of technetium, rhenium was chosen as a simulant because of previously established similarities in ionic radii and other chemical aspects. The glasses containing target Re concentrations varying from 0 to

* Corresponding author Tel.: +1-509-372-4964; Fax: +1-509-372-5997

E-mail address: john.mccloy@pnnl.gov

10,000 ppm by mass were synthesized in vacuum-sealed quartz ampoules to minimize the loss of Re by volatilization during melting at 1000 °C. The rhenium was found to be present predominantly as Re^{7+} in all the glasses as observed by X-ray absorption near-edge structure (XANES). The solubility of Re in borosilicate glasses was determined to be ~3,000 ppm (by mass) using inductively coupled plasma-optical emission spectroscopy (ICP-OES). At higher rhenium concentrations, some additional material was retained in the glasses in the form of alkali perrhenate crystalline inclusions detected by X-ray diffraction (XRD) and laser ablation-ICP mass spectrometry (LA-ICP-MS). Assuming justifiably substantial similarities between Re^{7+} and Tc^{7+} behavior in this glass system, these results implied that the processing and immobilization of ^{99}Tc from radioactive wastes should not be limited by the solubility of ^{99}Tc in borosilicate LAW glasses.

Keywords: radioactive waste; technetium; rhenium; inductively coupled plasma; borosilicate glass

1. Introduction

The Hanford site in Washington is home to approximately 2.1×10^{11} m^3 (~5.5×10^7 gallons) of radioactive and chemically hazardous wastes stored in 177 underground tanks.[1] The wastes were generated as a result of 45 years of plutonium production in support of the nation's defense programs. The current plan is to separate the tank wastes into high-volume, low-activity waste (LAW) and low-volume, high-level waste (HLW) fractions, which will then be vitrified into separate glass waste forms for long-term storage. The LAW vitrification product will be

stored at the on-site integrated disposal facility while HLW glass will be transported to a deep geologic repository when such a location becomes available.[1]

The LAW at Hanford primarily consists of aqueous solutions containing Na^+, K^+, $Al(OH)_4^-$, Cl^-, F^-, NO_2^-, NO_3^-, OH^-, CO_3^{2-}, and organics as well as other minor ionic species, including radionuclides. Some of the main radionuclides found in Hanford LAW include technetium-99 (^{99}Tc), iodine-129 (^{129}I), cesium-137 (^{137}Cs), and strontium-90 (^{90}Sr). The long-lived ^{99}Tc and ^{129}I radionuclides are a matter of concern in comparison to ^{137}Cs and ^{90}Sr, which are short-lived and predominantly fractioned into HLW. According to a recent estimate, the Hanford site tanks contain ~25,000 Ci (~1,500 kg) of ^{99}Tc and ~32 Ci (~180 kg) of ^{129}I.[2] The current flowsheet calculations estimate that more than 90% of the ^{99}Tc inventory in the tanks will be immobilized in the LAW glass whereas only about 20% of the ^{129}I inventory will be incorporated into the LAW glass.[3] According to the performance assessments conducted to provide guidance for the storage and disposal project for Hanford LAW, ^{99}Tc is the major dose contributor during the first 30,000 years following disposal.[2, 4]

The major environmental concern with ^{99}Tc is its high mobility in addition to a long half-life (2.1×10^5 yrs). The highly soluble TcO_4^- does not adsorb well onto the surface of minerals and, thus, migrates nearly at the same velocity as groundwater.[5, 6] On the other hand, the primary concern with processing the Tc-containing waste into a glass is its volatility and hence the low retention.[7] Other sources of Tc-loss may include entrainment with volatilized solvent, formation of aerosols, dust particles in scrubber systems, and other similar sources that can be partially mitigated by engineering systems and recycling.[8] According to the current flowsheet for the Hanford vitrification process, >90% Tc is being estimated to be immobilized in the LAW glass based on the assumption that all the Tc collected through off-gas is recycled back to the

vitrification system. Some recent studies have focused on the issue of Tc volatility from the glass melt with and without cold cap.[9] Partitioning to the molten salt phase has also been suggested as a mechanism for low retention of Tc in the glass.[10] Volatilization of Tc can occur from the salt layer more readily than from the glass, especially if sulfate is present.[11] Therefore, it is critical to understand the mechanism of Tc retention in or escape from glass melt for the management of Tc in LAW vitrification. One of the potential factors that can affect the retention of Tc is its solubility in LAW glass. To the best of authors' knowledge, there is no published data on the solubility of Tc in borosilicate glasses for nuclear waste vitrification. The ultimate goal of the present study is to determine the solubility of Tc in a borosilicate glass for vitrification of Hanford LAW.

Rhenium (Re) has been the preferred non-radioactive Tc surrogate material over other candidates such as Mn or W, because of rhenium's similarities to technetium in chemistry, ionic size, speciation in glass, and other aspects.[8] Although, many studies have reported some differences in the reduction potential of the heptavalent species in Re and Tc,[12-15] the similarities between Re and Tc, as well as ReO_4^- and TcO_4^-, overwhelmingly argue for its utility in obtaining preliminary data which in a non-radioactive environment which can later be corroborated using studies with Tc itself.[15, 16] Rhenium compounds should be chemically similar to those expected for technetium in LAW simulants ($KTcO_4$) as well as those in liquid ($CsTcO_4$, $NaTcO_4$, and $KTcO_4$) and vapor [Tc_2O_7 and $TcO_3(OH)$] phases during vitrification.[8] This paper reports the results on the solubility of Re in a simulated waste glass specifically designed for one of the Hanford's representative LAW streams. The testing with radioactive Tc is in progress and the results will be present in a follow-on article.

2. Experimental

In order to determine the true solubility of Re in a borosilicate glass, the volatilization loss of Re species above the melt was eliminated by heat treating the glasses mixed with Re source material in vacuum sealed (~10^{-4} Pa) fused quartz ampoules so that even the Re species in the gaseous phase would still remain in contact with the glass melt surface. This paper describes the unique experimental procedure designed to perform these solubility experiments along with the results obtained from various characterization techniques in order to quantify the solubility and retention of rhenium in the glasses.

2.1 Glass synthesis

2.1.1 Synthesis of baseline glass

The borosilicate LAW glass with nominal composition shown in Table 1 was synthesized with the melt-quenching technique and is termed the *baseline* glass. The *baseline* glass, or the glass without any Re additions, was made in a large batch from the appropriate amount of oxides (MgO, Al_2O_3, H_3BO_3, SiO_2, Cr_2O_3, ZrO_2, TiO_2, ZnO, Fe_2O_3), carbonates ($CaCO_3$, Na_2CO_3, K_2CO_3) and sulfates (Na_2SO_4). The glass batch was homogenized in a vibrating agate mill and melted in a platinum alloy crucible at 1200 °C for 1 h. The resulting glass was quenched on a steel plate and crushed inside a tungsten carbide mill within a vibratory mixer yielding a fine glass powder.

Table 1. Compositions of the glasses (oxide basis).

Re-conc. (ppm)	Unit	SiO_2	Al_2O_3	B_2O_3	Na_2O	CaO	Fe_2O_3	Cr_2O_3	K_2O	MgO	SO_3	TiO_2	ZnO	ZrO_2	Re_2O_7	$KReO_4$
0	Mass%	45.30	6.10	10.00	21.00	2.07	5.50	0.02	0.47	1.48	0.16	1.40	3.50	3.50	-	-
("baseline")	Mol.%	50.39	4.00	9.60	22.64	2.47	2.30	0.01	0.33	2.45	0.13	1.17	2.87	1.63	-	-
100	Mass%	45.29	6.10	10.00	21.00	2.07	5.50	0.02	0.47	1.48	0.16	1.40	3.50	3.50	-	0.016
	Mol.%	50.39	4.00	9.60	22.64	2.47	2.30	0.01	0.33	2.45	0.13	1.17	2.87	1.63	-	0.004
1,000	Mass%	45.23	6.09	9.98	20.97	2.07	5.49	0.02	0.47	1.48	0.16	1.40	3.49	3.00	-	0.16
	Mol.%	50.37	4.00	9.60	22.64	2.47	2.30	0.01	0.33	2.45	0.13	1.17	2.87	1.63	-	0.04
2,500	Mass%	45.12	6.08	9.96	20.92	2.06	5.48	0.02	0.47	1.47	0.16	1.39	3.49	2.99	-	0.39
	Mol.%	50.34	3.99	9.59	22.62	2.46	2.30	0.01	0.33	2.45	0.13	1.17	2.87	1.63	-	0.09
4,000	Mass%	45.02	6.06	9.94	20.87	2.06	5.47	0.02	0.47	1.47	0.16	1.39	3.48	2.98	-	0.62
	Mol.%	50.31	3.99	9.59	22.61	2.46	2.30	0.01	0.33	2.45	0.13	1.17	2.87	1.62	-	0.14
6,415	Mass%	44.85	6.04	9.90	20.79	2.05	5.45	0.02	0.47	1.47	0.16	1.39	3.47	2.97	-	0.99
	Mol.%	50.27	3.99	9.58	22.59	2.46	2.30	0.01	0.33	2.45	0.13	1.17	2.87	1.62	-	0.23
10,000	Mass%	44.60	6.01	9.84	20.67	2.04	5.41	0.02	0.46	1.46	0.16	1.38	3.45	2.95	-	1.55
	Mol.%	50.20	3.98	9.56	22.56	2.46	2.29	0.01	0.33	2.45	0.13	1.17	2.86	1.62	-	0.36
6,407	Mass%	44.92	6.05	9.92	20.83	2.05	5.45	0.02	0.47	1.47	0.16	1.39	3.47	2.98	0.83	-
	Mol.%	50.33	3.99	9.59	22.62	2.46	2.30	0.01	0.33	2.45	0.13	1.17	2.87	1.63	0.12	-

2.1.2 Synthesis of rhenium containing glasses

Since the predominant form of Tc in the dried Hanford LAW will most likely be an alkali pertechnetate,[8] we chose $KReO_4$ (Alfa Aesar, 99% metal basis, Re 64 mass%) as the primary source of Re for our experiments. In one experiment, Re_2O_7 (NOAH Tech., 99.99%, -4 mesh) was used as an alternative Re-source in order to assess the influence of different Re precursors (with the same oxidation state) on the Re solubility in glass under a controlled environment. The concentration of Re added to the baseline glass was varied between 0 and 10,000 ppm (see Table 1), defined as parts per million, by mass, of Re atoms in the glass. The fractions of the other components in the glasses with Re additions were kept in constant ratios with those in the baseline glass, renormalized to the remaining mass fraction after accounting for the Re-source.

The LAW glass powder (as obtained from the experimental procedure mentioned previously) and the specified amount of Re-source powder were mixed in the tungsten carbide mill to prepare a mixture with a final batch size of 50 g, of which 30 g was used for the Re-solubility study, while the remaining 20 g was set aside for additional experiments. The glass frit was prepared this way so that the sulfate would be well-mixed and soluble in the glass and so that the Re-source powder could be well-mixed within the glass and captured by the glass powder sintering at the maximum allowable solubility. It should be noted that Re-free LAW glass powder (0 ppm Re) was also re-melted under similar conditions and will be considered as the *baseline experiment* in this study.

Each 30 g glass powder batch was placed into a flat-bottomed fused quartz tube and a fused quartz end cap was then inserted into the tube (Fig. 1). The tube was then connected to a vacuum system with compression fitting and evacuated. Once the pressure was ~10^{-4} Pa (~10^{-6} Torr), the tube was sealed with an oxygen-propane torch. This vacuum sealed tube will hereafter

be referred to as the *ampoule*. The ampoule containing powdered glass batch was inserted in the furnace pre-heated at 700 °C. The temperature of the furnace was increased from 700 °C to 1000 °C at a heating rate of 5 ^{o}C min^{-1} followed by a dwell of 2 h at 1000 °C to ensure the complete melting of glass batch. Higher temperatures were attempted initially, but there were concerns with 1) dissolving the fused quartz due the high sodium content and thus changing the batch chemistry and 2) having the Re compound attack the ampoule wall. At the end of the heating time, the ampoule containing glass melt was finally quenched in air within a stainless steel canister.

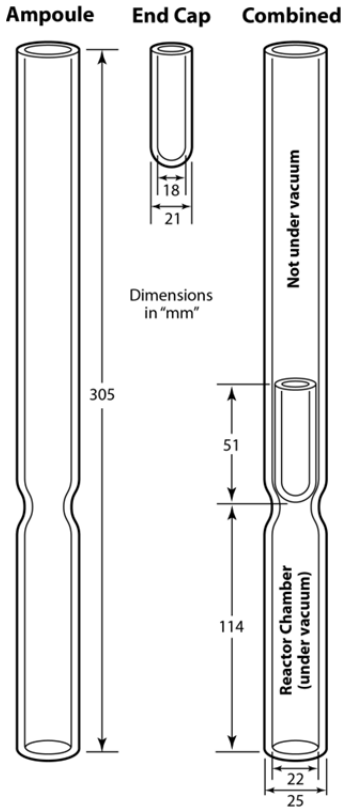

Fig. 1. Schematic of sealed ampoule for glass making. The glass batch is placed in the bottom portion of the combined ampoule on the right.

2.2 Characterization of glasses

2.2.1 X-ray diffraction (XRD)

All of the glasses and selected crystalline samples were analyzed with a Bruker® D8 Advance (Bruker AXS Inc., Madison, WI) XRD equipped with a Cu K_α target at 40 kV and 40 mA. The instrument had a LynxEye™ position-sensitive detector with a scan range of 3° 2θ. Scan parameters used for sample analysis were 5–110° 2θ with a step of 0.015° 2θ and a 0.3-s dwell at each step. In order to obtain higher resolution diffraction data to resolve any additional weak crystalline peaks, the glass samples with Re concentration of 10,000 ppm were analyzed in the 2θ range of 10–60° with a step of 0.015° 2θ and a 2.5-s dwell at each step. For all scans, JADE 6© (Materials Data, Inc., Livermore, CA), software was used to identify phase assemblages.

2.2.2 Scanning electron microscopy-energy dispersive spectroscopy (SEM-EDS)

The microstructure was analysed on select samples with a JEOL scanning electron microscope (SEM, JSM-5900, JEOL Ltd., Tokyo, Japan) equipped with a tungsten filament and a Robinson backscatter electron detector. Additionally, an EDAX Si-drift detector was used to conduct energy dispersive spectrometry (EDS, Apollo XL, AMETEK, Berwyn, PA) for dot mapping. A 20 kV acceleration voltage was used for all imaging and analysis. Note that the baseline glass contained both Si (K_α = 1.739 keV) and Zn (K_α = 8.628 keV) with X-ray emission energies comparable to Re M_α (1.842 keV) and L_α (8.650 keV) X-rays; EDS could not be reliably used for semi-quantitative Re determination.

2.2.3 X-ray Absorption Near Edge Structure (XANES) spectroscopy

For most of the glasses, XANES data were collected at the Re L_2-edge (11959 eV) with the Stanford Synchrotron Radiation Laboratory 11-2 beamline using a Si (220) double crystal

monochromator. The harmonic content of the beam was reduced by detuning the monochromator by 50%. The powdered glass samples were contained in aluminum holders sealed with Kapton tape. Data were recorded in transmission mode using Ar-filled ion chambers or in fluorescence mode using a 32-element Ge detector and were corrected for detector dead time effects. Data analysis was performed by standard procedures[17] with Artemis software.[18] The Re XANES spectra were also analysed by principal component analysis with SixPack software.[19]

Reference spectra for ReO_2, ReO_3 and $KReO_4$ were used for data fitting. The data fitting was based on a non-linear least squares method and was performed in the locally written program "fites." Six parameters were used in the fit: the amplitudes of the three standards, one global energy shift, and slope and offset (linear correction to account for differences in background correction). Data were fitted between 11940 and 12040 eV and the data resolution is estimated to be 6.5 eV based on the width of the white line at the Re L_2-edge. The actual improvement of the fit due to incorporation of the ReO_2 and ReO_3 standards was examined with an F-test by comparing χ-squared with and without the ReO_2 standard. The null hypothesis in the F-test was that including the additional rhenium oxide spectrum did not improve the fit, and a probability of F, or p(F), is less than 0.05 indicating that inclusion of a fraction of the particular rhenium oxide spectrum improved the fit to better than two times the standard deviation. No F-test was performed on the $KReO_4$ standard as this was the main component in all spectra. Additional data on the goodness-of-fit are included in the **Supplementary Information**.

2.2.4 Laser ablation-inductively coupled plasma-mass spectrometry (LA-ICP-MS)

The LA-ICP-MS was used to analyze the chemical nature of bulk (polished) glass samples and to detect the presence of any crystalline/metallic Re inclusions in the samples. Glass samples were embedded in resin and polished to a 1-μm finish prior to LA-ICP-MS analysis.

The polished glass samples were mounted in a laser system sample holder (UP-266 Macro, New Wave Research Inc, USA) and coupled to a quadrupole ICP-MS (PQ Excell, VG Elemental, England). The rhenium sensitivity for ^{187}Re was ~1,000 counts per second per ppm (cps/ppm), based on a raster ablation with a 20-μm diameter laser spot, rising to ~8,200 cps/ppm with a 70-μm diameter laser ablation spot. These values were determined by ablating the National Institute of Standards and Technology (NIST) "50 ppm" trace elements in a Standard Reference Material (SRM) 612 glass standard.[20] Additionally, comparative measurements were made with the "500 ppm" trace elements in glass standard SRM 610.[20] These standards are not certified for Re concentration, but have been measured by dissolution methods and reported in the literature, with SRM glass number 612 having 6.57 ppm Re content and SRM glass number 610 having 49.9 ppm Re content.[21]

Rhenium distribution studies on the fabricated glasses were performed by ablating a grid of 100 spots, typically 0.5 × 0.5 mm total area, repeating the measurement over five to six sites across a sample and averaging the data. Single point feature studies such as probing intact gas bubbles were performed by allowing the laser to ablate into the glass to reach the subsurface feature of interest. For these types of analysis the ICP-MS was run in time-resolved analysis mode. More details on the depth profiling with LA-ICP-MS is provided in the **Supplementary Information**.

During Re analysis, the laser was scanned over the surface of the sample in a raster pattern (scan speed 25 μm/sec) for a period >3 minutes while the ICP-MS collected the intensities of target analytes averaged over three one-minute blocks. Similar laser ablation measurements were performed on the SRM 612 and/or SRM 610 standards under identical conditions and the Re levels in the test glasses were estimated by relative signal ratios assuming

the reported Re concentration in these standards as stated above. These SRM glasses were run before and often in the midst of the unknown Re concentration glasses each day that the LA-ICP-MS was run to account for variations in set-up, laser power drift, and other uncontrolled factors.

2.2.5 Inductively coupled plasma-optical emission spectroscopy (ICP-OES)

The ICP-OES was employed to quantify the Re concentration (irrespective of its solubility or retention) in the as-synthesized glasses. Fragments of glass samples weighing 20–40 mg were dissolved in 2 mL of concentrated ultra-pure (Optima Grade, Thermo-Fisher Scientific, Canada) hydrofluoric acid (HF) by mild heating (no boiling) at ~ 100 °C on a hot plate in 15 mL, capped perfluoro-alkoxy (PFA) crucibles for 2–3 hours. This procedure left a small amount of undissolved white powder. The bulk Si was then slowly evaporated off with the HF until it was completely dry. Then, 2 mL of concentrated hydrochloric acid (HCl) was added and evaporated. Then, a mixture of 0.5 mL HCl and 1.5 mL HNO_3 was added to the PFA crucible and heated gently for 1 h.

Once the glass dissolution was completed and the crucible was allowed to cool down to room temperature, the contents of each crucible and 18.2 Megaohm deionized water rinses were transferred to weighed test tubes yielding ~10 g of total solution. From this solution, a weighed volume was further diluted by a factor of ten using 1% by mass HNO_3 to prepare the final solution for ICP-OES analysis (ICAP 6500 Duo, Thermo-Fisher Inc., England). Typical sample Re concentrations were in the range 0.1–2 ppm after final dilution. Quantitative analysis was performed by generating a calibration curve at three Re emission wavelengths (197.3, 221.4 and 227.5 nm), by serial mass dilution of a Re 999 ± 2 ppm solution concentration standard (Inorganic Ventures, USA) in 2% by mass HNO_3. The calibration plots for all three wavelengths showed a linearity of 0.99 or better.

3. Results and discussion

3.1 Structural characterization of glasses

Melting the initial glass frit at 1200 °C for 1 h was sufficient to produce a homogenous baseline (no Re) LAW glass with dark brown color. The absence of crystalline inclusions was also confirmed by XRD and SEM analyses. The glass transition temperature (T_g) determined from the DSC thermograph for this glass was ~530 °C while no exothermic crystallization curve could be observed until 1100 °C (see **Supplementary Information**). Magic angle spinning-nuclear magnetic resonance (MAS-NMR), Fourier transform infrared (FTIR) spectroscopy, and Raman spectroscopy were also conducted to characterize glasses as a function of Re source additions. Details of these measurements can be found in the **Supplementary Information**. In general, these techniques showed a glass composed of primarily Q^2 and Q^3 structural units, with Si, Al, or B tetrahedra, due to the large sodium content causing non-bridging oxygens. Aluminum is 4-coordinated, and boron is largely 3-coordinate with some 4-coordinated. Rhenium source additions did not appear to have clear effects on the glass structure as evidenced by MAS-NMR, FTIR, and Raman spectroscopy. Thus at the concentrations that remain in glass, the Re appears to be neither a glass-former nor a strong glass modifier. As discussed below, it likely exists in isolated ReO_4^- anions in the interstices of the glass network.

3.2 Crystallinity in Re glasses

The rhenium-containing glass melts exhibited different physical and chemical features during the glass synthesis depending on their initial rhenium concentration. A brief account of visual observations that were made during synthesis of these glasses along with the results obtained from characterization of these glasses by XRD and SEM-EDS is presented below.

Remelting of the baseline glass (with 0 ppm Re) in the quartz ampoule resulted in a cylindrical shaped glass ingot, which cracked and shattered into small pieces upon cooling due to the stresses from a thermal expansion mismatch between the glass and fused quartz. No significant interfacial reactions between glass melt and walls of quartz ampoule were observed. The addition of Re (100–2500 ppm) in the baseline glass with $KReO_4$ as its source resulted in amorphous glasses as revealed by XRD analysis (Fig. 2). Further increase in the Re concentration to ~6400 ppm (source: $KReO_4$) led to the formation of a separate low viscosity liquid phase (estimated to be < 0.1 Pa s) floating on top of the glass surface during cooling that gradually solidified to a white-colored superficial powdered layer. The XRD analysis of this superficial white powder revealed its highly crystalline nature with the dominance of alkali perrhenates along with some minor phases, notably sulfates (Fig. 3), while the glass itself remained amorphous (Fig. 2). Similar observations were made for the glass with 10,000-ppm Re (source: $KReO_4$) where a low viscosity liquid phase floated on the top of the glass and gradually solidified to form a highly crystalline white powder on the surface of the solidified glass. This powder was identified as having a dominance of $NaReO_4$ phase along with some minor phases including $KReO_4$ plus SiO_2, the latter likely due to impurity addition from the walls of quartz ampoule (Fig. 3).

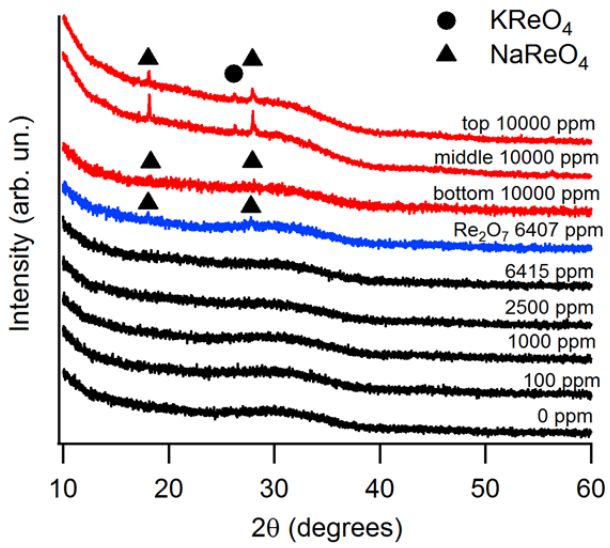

Fig. 2. Powder XRD of glasses.

Unlike the 6,415 ppm (source: $KReO_4$) sample which exhibited no crystalline peaks, the glass obtained with the 10,000 ppm Re concentration showed evidence of $KReO_4$ and $NaReO_4$ phases. In order to obtain an insight into the distribution of crystalline inclusions in the sample, the glass was cut in three sections (bottom, middle, top) relative to the cooled white salt phase. The powder XRD analysis on three different parts of the glass sample revealed the heterogeneous distribution of crystalline inclusions of alkali perrhenates in the sample as the top and middle sections of the glass exhibited the strong crystallinity while the bottom section of glass was only weakly crystalline (Fig. 2). The explanation for this spatial segregation of crystalline phases is not clear, but it may be related to the transport of supersaturated rhenium towards the surface in bubbles where eventually forms a surface salt phase.

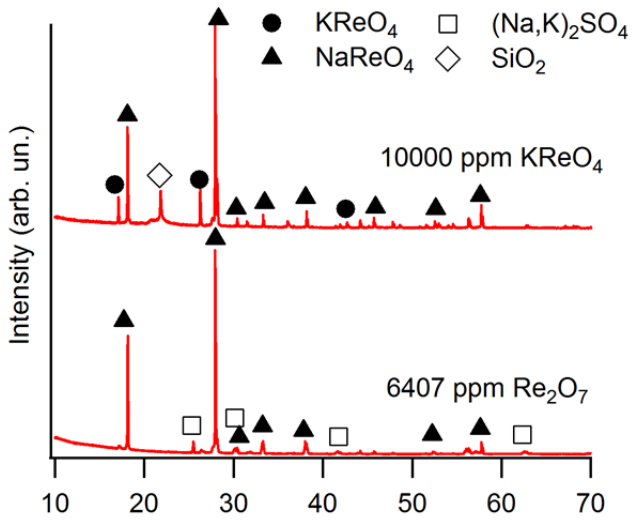

Fig. 3. XRD of white salt from melt surface.

With respect to the synthesis of glass with Re_2O_7 as the rhenium source and Re concentration of ~6,400 ppm, we did not observe any significant interaction between the glass melt and walls of the quartz ampoule. From XRD analysis, the resulting glass did show Re-containing crystalline phases (Fig. 2) similar to the 10,000 ppm $KReO_4$ sample. Also similar to its $KReO_4$ containing counterpart, a low-viscosity liquid phase was observed floating on the top of the glass surface that gradually solidified to white-colored superficial powdered layer. The XRD analysis of the white powder revealed its crystalline nature (Fig. 3) with $NaReO_4$ as the major crystalline phase with minor phases of $KReO_4$ and alkali sulfate. The bottom part of the quartz ampoule cracked after a few minutes of air-quenching due to the thermal stresses, leading to the release of a plume of gas in the canopy hood above the furnace.

The SEM micrographs of the white powder at different locations on the glass surface illustrate their highly crystalline microstructure with dendritic morphology as shown in Fig. 4. The EDS elemental dot mapping of the dendritic crystals found on a fracture surface reveals the dominance of sodium, sulfur and rhenium in these crystals (Fig. 5). It is noteworthy that,

although the crystalline microstructure of the white powders is enriched in sulfur along with Re and Na, we did not observe any Re-S containing phase during the XRD analysis (Fig. 3). Additionally, the EDS confirms that the sulfur is associated with sodium (probably Na_2SO_4 with some K), while the rhenium appears to be mostly associated with potassium (probably $KReO_4$ with some Na). It is likely that the perrhenate and sulfate salts were intimately mixed in the low viscosity liquid on top of the glass and then deposited in the crack upon cooling where they formed separate crystalline phases.

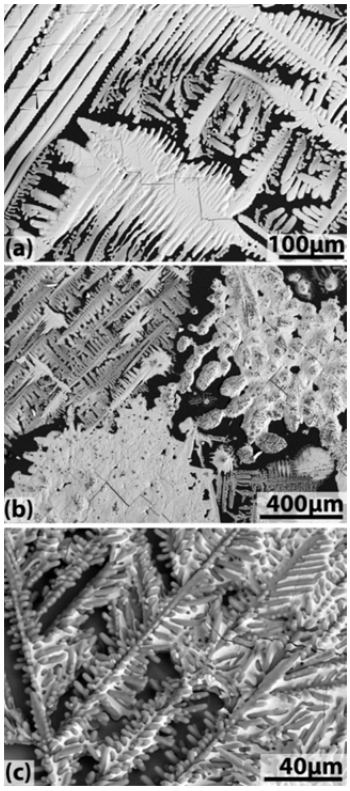

Fig. 4. SEM micrographs of salt phase on the top (a,b) and fracture surfaces (c) of the Re_2O_7 glass.

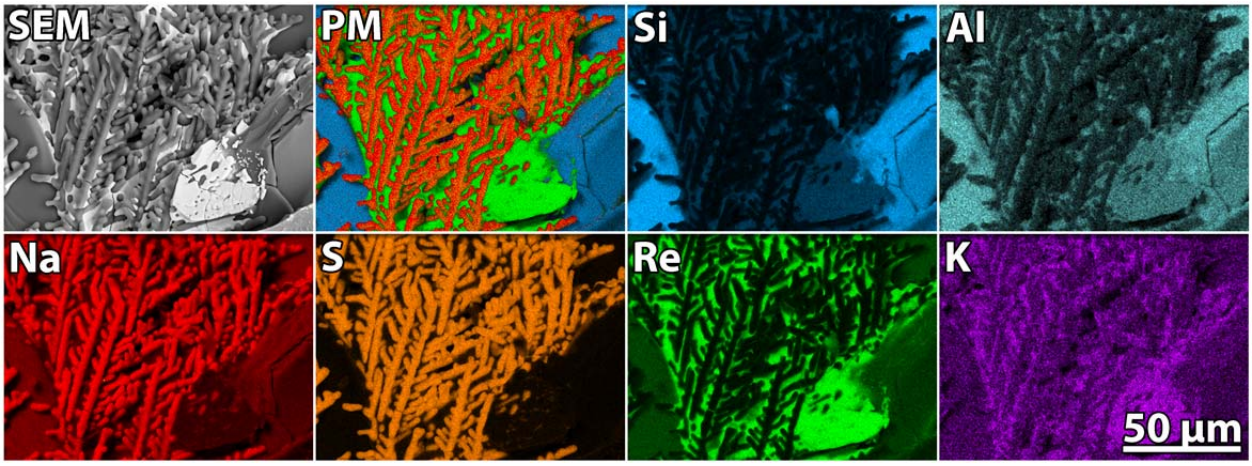

Fig. 5. Backscattered electron SEM micrographs, phase map (PM), and elemental distribution (Si, Al, Na, S, Re, and K) for dendritic crystals found on the fracture surface of the Re_2O_7 glass (based on results from EDS analysis).

3.3 Rhenium valence and coordination in glasses

The Re-XANES spectra of the studied glasses are presented in Fig. 6 while the fitting results are presented in Table 2. Fitting results of glasses at the two extremes of Re loading are shown in Fig. 7. The F-test revealed that the ReO_2 and ReO_3 standards do not significantly improve the fit for any of the glass samples since p(F) in all cases is greater than 0.05. However, for glass prepared with 10,000 ppm $KReO_4$, the amount of Re^{7+} is not within two standard deviations of 1.0, and it is possible that other, lower valent Re species are present in this sample. These results are in general agreement with those reported by Lukens *et al.*[12] which predicts only Re^{7+} at these oxygen fugacities. However, the 10,000 ppm result in this work suggests that this sample may contain other Re species as well, but even if so, the Re^{7+} accounts for 90% of the Re species and so is of primary importance.

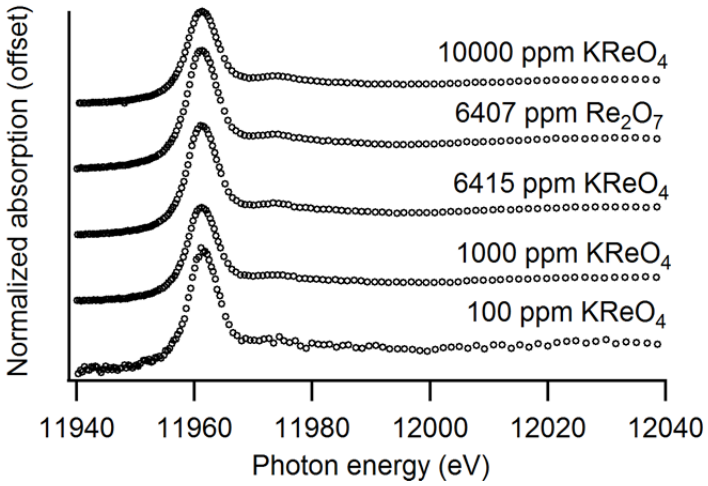

Fig. 6. XANES results for some of the glasses (data are offset for clarity).

Table 2. XANES fitting results.

ppm Re target	Re source	ReO_2*	p(F)†	ReO_3*	p(F)^	$KReO_4$*
100	$KReO_4$	0.0(2)	1.00	0.0(2)	1.00	1.0(1)
1000	$KReO_4$	0.03(9)	0.77	0.03(8)	0.72	0.94(5)
6415	$KReO_4$	0.04(7)	0.61	0.04(6)	0.60	0.93(4)
10000	$KReO_4$	0.09(6)	0.23	0.03(5)	0.63	0.89(3)
6407	Re_2O_7	0.05(7)	0.55	0.05(6)	0.51	0.91(4)

* Number in parentheses is the standard deviation and is in the same units as the digit preceding it.
†p(F) is the probability that the improvement in the fit due to adding this component is due to random error. The component can be considered present in the sample if p(F) is less than 0.05.

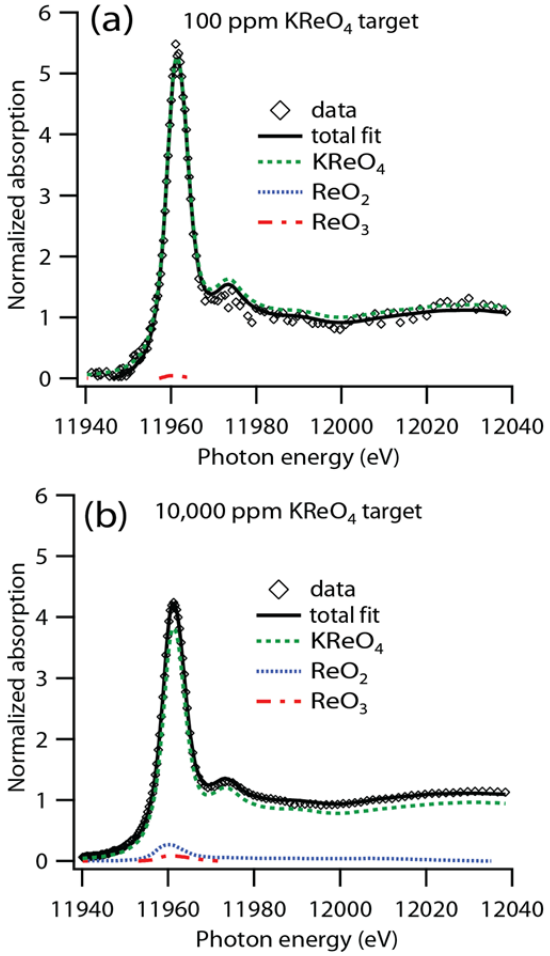

Fig. 7. Fitted XANES data for (a) 100 ppm and (b) 10,000 ppm $KReO_4$ glasses.

3.4 Rhenium solubility in glasses

In agreement with the XRD results (Fig. 3), the presence of rhenium-rich crystalline inclusions in the glass with target Re concentration 6,415 ppm (source: Re_2O_7) was confirmed by LA-ICP-MS data as presented in Fig. 8. A sharp increase in the intensity counts for ^{187}Re in Fig. 8 imply that the laser beam ablated a Re-containing crystalline inclusion that was likely in the form of $NaReO_4$ as detected by XRD analysis (Fig. 3). The depth profiling process used to distinguish bubbles from inclusions is described in the **Supplementary Information**.

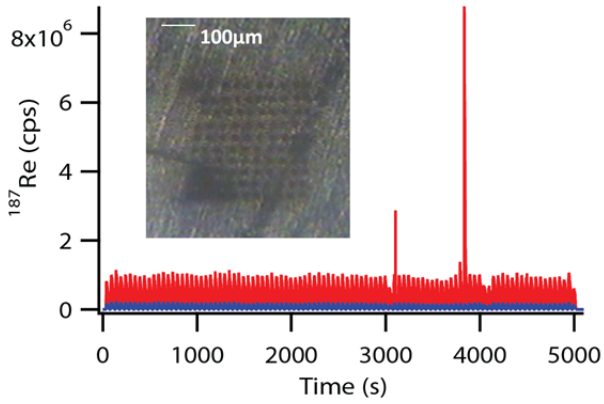

Fig. 8. LA-ICP-MS signal versus time, showing the presence of Re inclusions in the 6407 ppm Re glass made with Re_2O_7. Inset shows typical ablation pattern. The blue background signal (very low counts) is ^{96}Zr for comparison.

Quantitative ICP-OES results are shown in Table 3. Each glass was sampled at least twice and up to six times where various locations in the glass ingot were studied. Heterogeneity in the Re_2O_7 glass and 10,000 ppm $KReO_4$ glass was further confirmed by ICP-OES taken from different regions of the sample (top, middle, or bottom) (Fig. 9). ICP-OES analysis on the different pieces of glass revealed the higher concentration of rhenium in the top and middle parts of the glass sample in comparison to the bottom part of sample, which is in agreement with the result of higher crystallinity in the upper parts of the sample, and may be due to details of the transport of supersaturated rhenium to the surface of the melt such as in bubbles. Similar results

were obtained for the glass with 10,000 ppm of target Re concentration (source: $KReO_4$) as ICP-OES showed that the experimental rhenium concentration varied between 3000 and 4000 ppm in different pieces of glasses. These results are in good agreement with the XRD results presented in Fig. 3. By contrast, the 4,000 ppm (source: $KReO_4$) glass, produced last as a test case, showed relatively uniform Re concentration ~3000 ppm in all portions of the glass.

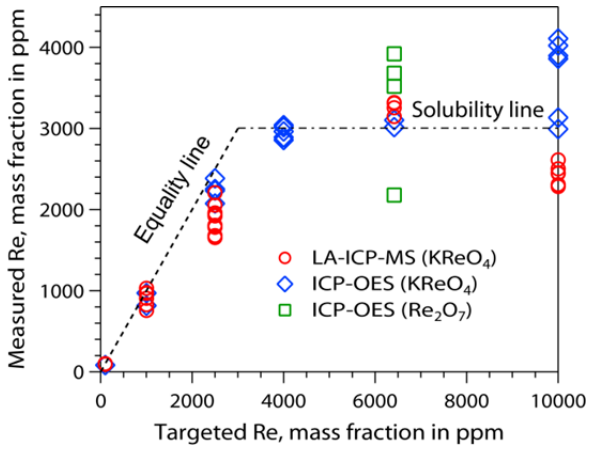

Fig. 9. Quantitative assessment of Re solubility in borosilicate glass

Table 3. ICP-OES results.

Target Re-conc. (ppm)	Re-Source	Location	Sample 1 (ppm)	Sample 1 Std. Dev (ppm)	Sample 2 (ppm)	Sample 2 Std. Dev (ppm)	Overall Mean (ppm)	Overall Std. Dev (ppm)	Inclusions*
100	$KReO_4$	n.t.	38	5	82	12	60	9	N
1000	$KReO_4$	n.t.	971	14	815	13	893	14	N
2500	$KReO_4$	Top	2075	67	2233	60	2154	64	N
		Bottom	2252	55	2385	47	2319	51	N
4000	$KReO_4$	Top	3042	41	3035	42	3038	41	N
		Middle	3013	44	2890	41	2952	43	N
		Bottom	2963	38	2856	40	2909	39	N
6415	$KReO_4$	n.t.	3016	23	3102	30	2059	27	N
10000	$KReO_4$	Top	3897	17	3859	21	3878	19	Y
		Middle	4021	19	4108	19	4065	19	Y
		Bottom	2993	12	9194	15	3064	14	Y
6407	Re_2O_7	Top	3681	25	3920	31	3801	28	Y
		Bottom	2178	19	3520	28	2849	24	Y

*"N" means that inclusions were not observed and "Y" means that inclusions were observed with XRD and/or LA-ICP-MS
n.t. – not tracked
Individual mean and standard deviation is determined from evaluation of four Re absorption lines for each sample. Overall mean and standard deviation is determined based on mean of the statistics of two independent samples. Data are rounded to the nearest ppm.

LA-ICP-MS data should be considered semi-quantitative, as proper quantification depends strongly on choosing a proper standard with the element of interest in the right range within a matrix that ablates similarly to the unknown sample.[22] The SRM glasses had very low Re concentration and gave unreasonably low numbers when used as the only source of calibration. Therefore, we chose to scale the LA-ICP-MS to the truly quantitative ICP-OES data as follows. The average value of the LA-ICP-MS results obtained using the SRM for 100, 1,000, 2,500, and 6,415 ppm $KReO_4$ samples was plotted against the average ICP-OES results for these same glasses and a scale factor of 1.798 was found to be reasonable to apply to the LA-ICP-MS individual values. As an independent check, two samples were analysed with electron probe microanalysis with wavelength dispersive spectroscopy (EPMA-WDS) and the quantified trend followed for variation in rhenium concentration in glasses is similar to that observed for the data obtained from ICP-OES and LA-ICP-MS (see **Supplementary Information**).

The ultimate solubility of Re in the borosilicate LAW glass (shown in Fig. 9) was determined as follows. The quantitative data from 4,000 ppm target (6 data points), 6,415 ppm target $KReO_4$ source (2 data points), and 10,000 ppm (2 data points with lower values) were averaged to obtain a value of 3,004 ppm. The justification for using the two lower values of the 10,000 ppm sample was that these points likely represented the bulk glass, whereas the two points with the higher Re measured values likely contained Re salt inclusions resulting in larger measured Re concentrations. The results of this analysis are shown in Fig. 9, which is considered the key result of our work. Here the "equality line" is shown representing where solubility is equal to retention of the Re, and the "solubility line" is shown representing the maximum incorporation of Re in the glass under these conditions without forming inclusions.

3.5 Rhenium retention in glasses

'Solubility' is defined as the concentration (in mass fraction) of Re at an established equilibrium between dissolved and atmospheric Re. However, the glass-making process generally does not allow the glass melt to reach equilibrium. While the portion of a component dissolved in the amorphous phase(s) may be unsaturated (i.e. below the solubility), a substantial portion may simultaneously exist in the form of inclusions (i.e. inhomogeneities). Therefore, the retention ratio is a dynamic quantity that depends on the glass-making conditions.[23] The retention ratio for of a particular element, *i*, is defined as

$$R_i = \frac{g_{i,r}}{g_{i,0}} \quad (1)$$

where $g_{i,0}$ is the target mass fraction of the element *i* (Re in present case) in the glass (i.e., the mass fraction of Re that would be present in glass if the total amount added with the feed were retained) and $g_{i,r}$ is the mass fraction of rhenium actually retained in the glass (here, as determined by ICP-OES analysis) and since $g_{i,0} \geq g_{i,r}$, $R_i \leq 1$. The difference between $g_{i,0}$ and $g_{i,r}$ is caused by losses to the atmosphere due to volatility and by the formation of surface salt phase enriched with Re. In an actual glass melter application, the retention is strongly influenced by volatility, which is enhanced when there is no cold cap present where unconverted feed covers at least part of the melt surface. Fig. 10 presents the retention ratio for Re in the investigated glasses. The following observations can be made from the obtained results:

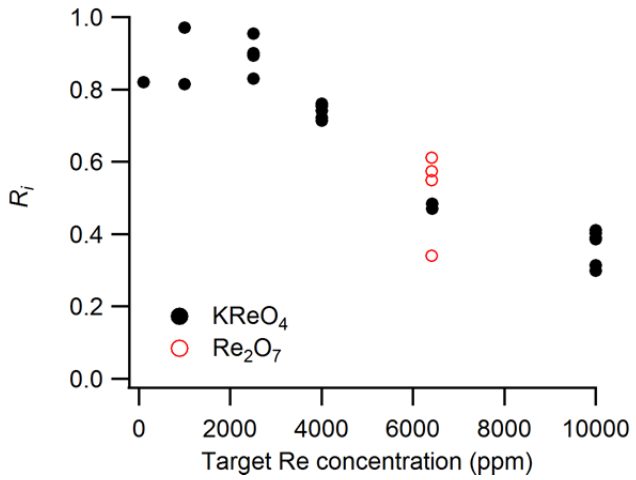

Fig. 10. Retention ratio, R_i, as a function of Re source input concentration.

- The Re concentration in glasses as obtained from ICP-OES varies almost linearly with the target Re concentration in the range of 100–2500 ppm as shown in Fig. 9. This shows that most of the rhenium (80–90%) added to the borosilicate glasses has been retained, the rest presumably being lost to volatilization. Further, the absence of any crystalline inclusions in these glasses confirms that at least up to 2,500 ppm Re concentration, retention ≤ solubility.
- An increase in the target Re concentration beyond 2,500 ppm led to the deviation in retention behavior from linearity. The maximum amount of Re retained in glass with target Re concentrations of 6,415 ppm (source: $KReO_4$) and 10,000 ppm were ~3,000 ppm and 3,000–4000 ppm, respectively. In the latter case, the 4,000 ppm was likely due to the presence of inclusions.
- The difference in Re-precursors (Re_2O_7 versus $KReO_4$) used in the glass melting showed its effect on Re-retention. Though two glasses were made at similar Re target levels of ~6400 ppm, the Re_2O_7 containing glass exhibited Re-concentration of 2,100–4,000 ppm (see Table 3), 3324±782 ppm by ICP-OES for four samples, while a much more repeatable ~3,000 ppm

Re, 3059±61 ppm by ICP-OES for two samples, was detected for $KReO_4$ glass (Fig. 9). Note that although fewer ICP-OES samples were investigated for the $KReO_4$ glass of this target Re concentration, multiple samples of LA-ICP-MS showed no indication of Re concentration fluctuations in the $KReO_4$ glass, whereas the Re_2O_7 glass showed evident inclusions by LA-ICP-MS (Fig. 8). It is unclear at present why the reactivity and resultant crystallinity of the Re_2O_7 glass is different, but it may be related to the segregation and interaction with a sulfate phase (Fig. 5).

- The significant spread in the values of retained Re concentration in glasses with target Re concentration > 6,500 ppm is due to the heterogeneous distribution of rhenium-rich inclusions in the glass matrix as has been already shown by XRD (Fig. 2).
- Some of the reduction in retention in the glass was due to formation of the white rhenium salt. Note that the salt layer was removed from the glass surface before analysing the glasses by ICP-OES and thus its Re content is not included in the soluble fraction of Re. The surface salts therefore represent a loss of retention of the target Re concentration.
- As is evident from Fig. 10, the retention ratio varied between 0.8 and 1 for glasses with target Re concentration ≤ 2,500 ppm while beyond that, R_i decreased considerably. The decreasing retention for low target Re concentrations can be attributed to volatility of rhenium from the glass melt and subsequent deposition on the walls of quartz ampoule. At higher Re target concentrations, Re salt could be lifted to the surface of the glass melt trapped in bubbles originating from the pores of the glass powder as it sinters or from redox reactions of Re or Fe. Tiny bubbles that remained in the glass after cooling were investigated by LA-ICP-MS. These bubbles did not contain Re (see **Supplementary Information**).

3.6 Redox and valence in Re and Tc

Although Re has been widely accepted as a surrogate for Tc, it is important to highlight some differences between the two species regarding their chemistry within the glass environment. Rhenium has a bulk silicate Earth abundance of 0.2 ppb and is the rarest of all the naturally occurring elements, apart from the noble gases,[24] thus there have been few comprehensive studies on its behavior outside of the geochemistry literature. The most prominent difference between Tc and Re is their contrasting reduction-oxidation (redox) behavior. Rhenium commonly occurs in the +7 oxidation state as Re_2O_7 or ReO_4^- (perrhenate ion) as well as in the +4 state in ReO_2 and the +6 state in ReO_3, whereas Tc occurs only in the 7+ or 4+ oxidation states.[8, 25]

Tc is more easily reduced from $Tc^{7+} \rightarrow Tc^{4+}$ compared to $Re^{7+} \rightarrow Re^{4+}$,[8] and thus it has been suggested that Re may not be a representative substitute for Tc under reducing conditions, at least in borosilicate LAW glasses.[12] In the vapor hydration test (VHT) used to assess chemical durability,[26] Tc has been observed to reduce to Tc^{4+} regardless of the starting Tc valence distribution, whereas Re^{7+} species remained dominant in the Re glass analogues.[27] Furthermore, Tc is enriched at the outer corroded gel-layer of amorphous silica while almost absent at the center, while Re concentrations are lower near the surface of comparable samples and approach that of unreacted glass near the center, thus highlighting the difference in mobility of Re and Tc in hydrothermal environments. Also, a series of recent melter tests suggest that the retention of Re is 8 to 10% higher than Tc for similar glasses.[28] Despite the lack of precise correlation in the redox of Re and Tc, the assumption of 100% Tc^{7+} and use of Re^{7+} as a surrogate should lead to a conservative estimate for solubility of Tc in an oxidizing environment, such as that present in the high nitrate feed environment at Hanford. Since Tc^{4+} is not nearly as mobile in water as Tc^{7+} (as

TcO_4^-) and not as volatile, the applicability of Re^{7+} data to Tc for these glasses should be reasonable. However, it should not be assumed that the solubility of Tc^{4+} (or Re^{4+}), which may be present in non-negligible quantities in other nuclear waste glasses, would be the same as the solubility of Tc^{7+} (or Re^{7+}).

According to the literature, volatility and retention of Tc and Re compounds in silicate and borosilicate glasses is strongly dependent on the oxidation state of the glass as well as on the feed chemistry.[8, 12] For example, Tc and Re tend to be more volatile when present as Tc^{7+}/Re^{7+} (TcO_4^-/ReO_4^-) than when present as Tc^{4+}/Re^{4+} (TcO_2/ReO_2). On the other hand, $KTcO_4$ and $KReO_4$ precursors are expected to produce lower Tc and Re volatilization at higher temperatures compared to Tc_2O_7 and Re_2O_7, respectively.[8, 29] Thus, the calculated or predicted maximum content of Tc/Re in glass in these literature studies is not the *solubility* but, rather, is the *retention* of Tc/Re in the glass after volatilization of these species during melting, the value of which should be significantly lower than the true solubility.

A number of studies have focused on the Tc or Re valences and concentrations in silicate or borosilicate glasses synthesized under various conditions, in order to determine the effect of the Tc/Re source starting material and redox on the solubility, retention, and volatility in glass.[12, 30-32] While the results from most of these studies seem to contradict each other, they actually provide a coherent description of the behavior of Re in silicate melts. Initial studies by O'Neill *et al*.[30] and Righter and Drake[31] suggested that Re dissolves in silicate melts as species with unusually low, valence states (Re^+ or Re^{2+}). Later work by Ertel *et al*.[32] demonstrated that these results were due to the presence of metallic Re "micronuggets" dispersed in the silicate melt. Using LA-ICP-MS, Ertl *et al*.[32] showed that Re actually dissolved in silicate melts with oxygen fugacities lower than 10^{-8} bar was present as Re^{4+} and Re^{6+}, but these species were only present

at 0.03 ppm concentrations in the presence of roughly 20 ppm of metallic Re. These results are consistent with those of Lukens *et al*.,[12] which spanned a much wider range of oxygen fugacities. At low oxygen fugacities, only metallic Re was observed in cooled glass samples, while at higher oxygen fugacities only Re^{7+} was observed[12] (XANES used in the cited study is not sensitive to the presence of small amounts of either Re^{4+} or Re^{6+} in the presence of a large excess of metallic Re or Re^{7+}).

The initial motivation for examining our samples using LA-ICP-MS were the previous reports that Re could concentrate in reduced metallic form in "micronuggets" in silicate melts which would skew the assessed solubility of a glass containing them.[32] Other than the evidence of inclusions, most probably sodium and potassium perrhenate, we did not see any evidence of the metallic "micronuggets" causing small but measurable fluctuations in Re concentration suggested by these previous authors, though these would be less likely to occur in our samples due to the specific redox conditions. Inclusions containing Re in our samples were indicated by very large excursions of Re concentration and were very spatially confined, which is phenomenologically different than the heterogeneous Re distribution reported by the geochemists.

An estimate for the solubility of Tc in borosilicate glass might be made based on a comparison of the solubility of Re measured in this study with the solubility of sulfur in borosilicate glass measured in various studies (~0.6 mol% SO_3 or ~3,000 ppm by mass S).[33] Using this value for sulfur solubility, the ppm mass value can be converted to a parts per million atoms (ppma) basis, and for the sodium borosilicate LAW glass with composition studied here, this equates to ~1,900 ppma for sulfur. The equivalent value for Re in our LAW glass assuming 3,000 ppm by mass solubility is ~333 ppma for rhenium, which is a six-fold reduction in

solubility compared to sulfur. One might speculate that this decreased solubility for Re compared to S, neither of which appear to participate in the glass network, is due to the much larger ionic radius of Re (S^{6+} = 43 pm, Re^{7+} = 67 pm, Tc^{7+} = 70 pm [34]). By this argument, then, Tc^{7+} should have an equivalent slightly lower solubility (in ppma) than Re^{7+}. Assuming the same ~333 ppma solubility for Tc^{7+} in this glass, its solubility should be ~1,500 ppm by mass.

From the standpoint of ultimate disposition of radioactive Tc in a glass waste form, a few considerations should be made. The required average maximum concentration of Tc to be immobilized in Hanford LAW glass can be estimated from 1) the estimated total Tc inventory in the underground tanks (~1,500 kg per Mann 2004[2]) and 2) the total estimated mass of LAW glass to be produced (527,838 metric tons per Certa et al 2011[1]). Assuming 100% retention of Tc and these numbers, the average Tc concentration in LAW glass is ~3 ppm by mass. Assuming that the solubility of Tc^{7+} on a per atom basis in glass is similar to that obtained for Re^{7+}, and assuming the redox state in LAW glass favors Tc^{7+}, solubility of Tc is orders of magnitude higher than current estimates of Tc concentrations in LAW, even when recycle loops are taken into account which theoretically ultimately result in 100% retention for volatile species. On the other hand, the apparent solubility of Re^{4+} in glass appears to be very low,[32] and if the same is true for Tc^{4+}, then the solubility of Tc in silicate glass depends greatly on the redox state of the melt. Additionally, as previously stated, Tc^{7+} is much more easily reduced than Re^{7+}, so Tc^{4+} may indeed be present in non-negligible concentrations in LAW glass, a possibility which should be verified experimentally. If Tc^{4+} is present in significant quantities, the solubility data obtained in the literature for Re^{4+} may not be relevant for Tc^{4+} since Re^{4+} is so difficult to form in realistic glass compositions, and another surrogate should be considered, such as Ti^{4+}, or preferably Ru^{4+}.[35] In Tc^{4+} the *d*-electrons are anti-bonding, which weakens the interaction

between oxide ligands and the metal, a situation more closely replicated by Ru which is adjacent to Tc on the periodic table. However, it is likely that Tc^{7+} will be the most important Tc valence for Hanford LAW glass due to the decomposition of nitrate and thus highly oxidizing environment in the melter.

The more important issue, then, becomes Tc retention. As shown by this study with Re, the retention can be substantially lower than the solubility even at low target concentrations due to kinetic factors such as volatility. Here future work will be needed to understand the details of the interaction between formation of a low-melting salt phase in LAW glass (which may contain pertechnetate, sulfate, chromate, chloride, iodide, nitrate, and nitrite along with various alkali metals), and volatilization from the cold cap where the slurry feed comes in contact with the melt pool. Here, previous work has shown that despite the estimated solubility of sulfate in borosilicate glass (~0.6 mol%), salt formation occurs at lower sulfate concentrations than its solubility.[36] Additionally, despite low concentrations of ^{137}Cs in LAW, which are less than that estimated for pertechnetate as most ^{137}Cs is partitioned to HLW, pertechnetate has been shown to enhance the volatility (and hence reduce the retention) of Cs,[8] possibly due to the formation of volatile $CsTcO_4$, resulting in additional safety concerns about the uncontrolled release of this short half-life, high dose contributor. Controlling the redox of the cold cap, then, to prevent formation of Tc^{7+} (and thus TcO_4^-) has been an area of intense research; however, decomposition of nitrites during vitrification of LAW glass will create highly oxidizing conditions in the melt, which may result in the formation of Tc^{7+} regardless of the initial oxidation state.[37]

4. Conclusions

We have determined that the solubility of rhenium in Na_2O-Al_2O_3-B_2O_3-SiO_2 simulated nuclear waste glass is ~3,000 ppm by mass when glass is equilibrated at 1000 °C for the

particular composition studied, a high sodium borosilicate representative of Hanford Low Activity Waste (LAW) glass. In all the glasses studied, the primary Re valence was +7, with a possible small fraction (<10%) of +4 in the glass when the maximum target of $KReO_4$ was added to the frit. We expect the solubility of Tc^{+7} to be substantially similar to that shown for Re^{+7} in this study, and a reduced scope test program is underway to verify this hypothesis. Given the high solubility of Re (and presumably Tc) in borosilicate glass, it is concluded that solubility is not a limiting factor in processing nuclear waste into glass given the currently estimated scenarios. Rather, it is the retention in glass that is the bigger concern, which is a more complex kinetic problem involving volatilization, phase separation, and complexation with alkali in the cold cap.

5. Acknowledgements

This work was supported by the Department of Energy – Waste Treatment & Immobilization Plant (WTP) Federal Project Engineering Division. The authors thank Orville (Tom) Farmer III for consultation regarding LA-ICP-MS, Prof. J.M.F. Ferreira from University of Aveiro, Portugal for FTIR and MAS-NMR, Juan (Jenny) Liu for EPMA-WDS, and Jaehun Chun for comments on the manuscript. Pacific Northwest National Laboratory is operated by Battelle Memorial Institute for the U.S. Department of Energy under contract DE-AC05-76RL01830. Portions of this work were supported by U.S. Department of Energy, Basic Energy Sciences, Chemical Sciences, Biosciences, and Geosciences Division, Heavy Element Chemistry Program and were performed at Lawrence Berkeley National Laboratory under Contract No. DE-AC02-05CH11231. Portions of this research were carried out at the Stanford Synchrotron Radiation Lightsource, a Directorate of SLAC National Accelerator Laboratory and an Office of

Science User Facility operated for the U.S. Department of Energy Office of Science by Stanford University.

References

1. P. J. Certa and P. A. Empey, River Protection Project System Plan, ORP-11242 Revision 6, Office of River Protection, US Department of Energy, Richland, WA, 2011.
2. F. Mann, Annual Summary of the Integrated Facility Performance Assessment for 2004, DOE/ORP-2000-19 Revision 4, CH2M HILL Hanford Group, Inc., Richland, WA, 2004.
3. J. H. Westsik, Hanford site secondary waste roadmap, PNNL-18196, Pacific Northwest National Laboratory, Richland, WA, 2009.
4. F. M. Mann and R. E. Raymond, Risk analysis supporting the decision of the initial selection of supplemental ILAW technologies, RPP-17675, Rev. 0, CH2M Hill Hanford Group, Richland, WA, 2003.
5. G. Shaw, ed., *Radioactivity in the terrestrial environment*, Elsevier, Oxford, UK, 2007.
6. W. Um, H.-S. Chang, J. P. Icenhower, W. W. Lukens, R. J. Serne, N. P. Qafoku, J. H. Westsik, E. C. Buck and S. C. Smith, *Environ. Sci. Technol.*, 2011, **45**, 4904-4913.
7. H. Lammertz, E. Merz and S. Halaszovich, *Mat. Res. Soc. Symp. Proc.*, 1985, **44**, 823-829.
8. J. G. Darab and P. A. Smith, *Chem. Mater.*, 1996, **8**, 1004-1021.
9. K. S. Matlack, I. S. Muller, I. L. Pegg and I. Joseph, Improved Technetium Retention in Hanford LAW Glass - Phase 1, VSL-10R1920-1, Vitreous State Laboratory, The Catholic University of America, Washington, DC, 2010.
10. D. S. Kim, L. M. Bagaasen, J. V. Crum, A. Fluegel, A. Gallegos, B. Martinez, J. Matyas, P. A. Meyer, D. R. Paulsen, B. J. Riley, M. J. Schweiger, C. W. Stewart, R. G. Swoboda and J. D. Yeager, Investigation of Tc migration mechanism during bulk vitrification process using Re surrogate, PNNL-16267, Pacific Northwest National Laboratory, Richland, WA, 2006.

11. D. S. Kim, C. Z. Soderquist, J. P. Icenhower, B. P. McGrail, R. D. Scheele, B. K. McNamara, L. M. Bagaasen, M. J. Schweiger, J. V. Crum, J. D. Yeager, J. Matyas, L. P. Darnell, H. T. Schaef, A. T. Owen, A. E. Kozelisky, L. A. Snow and M. J. Steele, Tc reductant chemistry and crucible melting studies with simulated Hanford Low-Activity Waste, PNNL-15131, Pacific Northwest National Laboratory, Richland, WA, 2005.

12. W. W. Lukens, D. A. McKeown, A. C. Buechele, I. S. Muller, D. K. Shuh and I. L. Pegg, *Chem. Mater.*, 2007, **19**, 559-566.

13. A. F. Armstrong and J. F. Valliant, *Dalton Trans.*, 2010, **39**, 8128-8131.

14. J. R. Dilworth and S. J. Parrott, *Chem. Soc. Rev.*, 1998, **27**, 43-55.

15. A. J. West, *Annu. Rep. Prog. Chem., Sect. A: Inorg. Chem.*, 2011, **107**, 173-182.

16. F. A. Cotton and G. Wilkinson, *Advanced Inorganic Chemistry*, John Wiley & Sons, New York, 1980.

17. D. C. Koningsberger and R. Prins, *X-Ray Absorption: Principles, Applications, Techniques of EXAFS, SEXAFS, and XANES*, John Wiley & Sons, New York, 1988.

18. B. Ravel and M. Newville, *Phys. Scripta*, 2005, **T115**, 1007-1010.

19. SIXPack (Sam's Interface for XAS Package) Documentation, http://ssrl.slac.stanford.edu/~swebb/spdocs/sixpack_documentation.htm.

20. K. P. Jochum, U. Weis, B. Stoll, D. Kuzmin, Q. Yang, I. Raczek, D. E. Jacob, A. Stracke, K. Birbaum, D. A. Frick, D. Günther and J. Enzweiler, *Geostand. Geoanal. Res.*, 2011, **35**, 397-429.

21. P. J. Sylvester and S. M. Eggins, *Geostand. Newslett.*, 1997, **21**, 215-229.

22. S. F. Durrant, *J. Anal. Atom. Spec.*, 1999, **14**, 1385-1403.

23. P. Hrma, Retention of halogens in waste glass, PNNL-19361, Pacific Northwest National Laboratory, Richland, WA, 2010.

24. H. S. C. O'Neill and H. Palme, *Composition of the silicate Earth: Implications for accretion and core formation. In The Earth's Mantle: Composition, Structure and Evolution*, Cambridge University Press, Cambridge, U.K., 1999.

25. J. M. MacKenzie and D. Canil, *Geochim. Cosmochim. Acta*, 2006, **70**, 5236-5245.

26. ASTM C 1663-09, *Standard test method for measuring waste glass or glass ceramic durability by vapor hydration test*, ASTM International, West Conshohocken, PA.

27. D. A. McKeown, A. C. Buechele, W. W. Lukens, D. K. Shuh and I. L. Pegg, *Environ. Sci. Technol.*, 2006, **41**, 431-436.

28. K. S. Matlack, I. S. Muller, R. A. Callow, N. D'Angelo, T. Bardacki, I. Joseph and I. L. Pegg, Improved technetium retention in Hanford LAW Glass-Phase 2, VSL-101R2260-1, Vitreous State Laboratory, The Catholic University of America, Washington, DC, 2011.

29. K. Schwochau, *Radiochim. Acta*, 1983, **32**, 139-152.

30. H. S. C. O'Neill, D. B. Dingwell, A. Borisov, B. Spettel and H. Palme, *Chem. Geol.*, 1995, **120**, 255-273.

31. K. Righter and M. J. Drake, *Earth Planet. Sci. Lett.*, 1997, **146**, 541-553.

32. W. Ertel, H. S. C. O'Neill, P. J. Sylvester, D. B. Dingwell and B. Spettel, *Geochim. Cosmochim. Acta*, 2001, **65**, 2161-2170.

33. R. K. Mishra, K. V. Sudarsan, P. Sengupta, R. K. Vatsa, A. K. Tyagi, C. P. Kaushik, D. Das and K. Raj, *J. Am. Ceram. Soc.*, 2008, **91**, 3903-3907.

34. R. D. Shannon, *Acta Crystallog. A*, 1976, **32**, 751-767.

35. H. D. Schreiber, F. A. Settle Jr, P. L. Jamison, J. P. Eckenrode and G. W. Headley, *JLCM*, 1986, **115**, 145-154.

36. J. D. Vienna, P. Hrma, W. C. Buchmiller and J. S. Ricklefs, Preliminary investigations of sulfur loading in Hanford LAW glass, PNNL-14649, Pacific Northwest National Laboratory, Richland, WA, USA, 2004.

37. P. A. Smith, J. D. Vienna and P. Hrma, *J. Mater. Res.*, 1995, **10**, 2137-2149.

Supporting Information

Rhenium solubility in borosilicate nuclear waste glass: implications for the processing and immobilization of technetium-99

Ashutosh Goel, Brian J. Riley, Martin Liezers, Michael J. Schweiger, Carmen P. Rodriguez, Charles F. Windisch, Jr., Pavel Hrma, Dong-Sang Kim, John S. McCloy*

Pacific Northwest National Laboratory, Richland, WA 99352, USA

Wayne W. Lukens, Jr.

Lawrence Berkeley National Laboratory, Berkeley, CA 94720, USA

Albert A. Kruger

DOE-WTP Project Office Engineering Division, Richland, WA 99352, USA

Experimental

Differential Scanning Calorimetry and the Glass Transition Temperature. The glass transition temperature (T_g) of the baseline LAW glass was obtained by loading 60 mg of glass powder into an alumina crucible and then into a differential scanning calorimeter (DSC-TGA, SDT Q600, TA Instruments, USA) in air, measuring from room temperature to 1100 °C at 10 ^{o}C min^{-1}. An empty alumina crucible was used as a reference.

Magic angle spinning nuclear magnetic resonance (MAS-NMR) spectroscopy. MAS-NMR was performed on a subset of the glasses to investigate the Si, Al, and B structure of the glasses. The

* Corresponding author Tel.: +1-509-372-4964; Fax: +1-509-372-5997

E-mail address: john.mccloy@pnnl.gov

^{29}Si MAS NMR spectra were recorded on a Bruker ASX 400 spectrometer operating at 79.52 MHz (9.4 T) with a 7 mm probe at a spinning rate of 5 kHz. The pulse length was 2 μs with a 60 s delay time and kaolinite was used as the chemical shift reference. The ^{27}Al MAS-NMR spectra were recorded at 104.28 MHz (9.4 T) with a 4 mm probe at a spinning rate of 15 kHz. The pulse length was 0.6 μs with a 4 s delay time and $Al(NO_3)_3$ was used as the chemical shift reference. The ^{11}B MAS-NMR spectra were recorded at 128.36 MHz (9.4 T) with a 4 mm probe at a spinning rate of 12 kHz. The pulse length was 3.6 μs with a 2 s delay time and H_3BO_3 was used as the chemical shift reference.

Fourier transform infrared spectroscopy (FTIR). Infrared spectra of the glasses were obtained using a Fourier spectrometer infrared spectrometer (FTIR, model Mattson Galaxy S-7000, USA). For this purpose glass powders were mixed with KBr in the proportion of 1/150 (by mass) and pressed into a pellet using a hand press. For both the background and sample collection, 64 scans were co-added with signal gain 1 with a 4 cm^{-1} resolution.

Raman spectroscopy. Raman spectra were acquired from bulk glass samples in a backscattering configuration with a Spex (Edison, NJ) Model 1877 Raman spectrometer equipped with Princeton Instruments (Trenton, NJ) liquid-nitrogen-cooled charge-coupled device detector. The 488.0-nm line of a Coherent (Santa Clara, CA) Innova 307 Ar^+ ion laser was used for excitation. The slit width was 400 μm and the exposure time was 15 s for most samples. Spectral acquisition and data analysis were performed using Princeton Instruments Winspec and Thermo Fisher Scientific (West Palm Beach, FL) Grams/32AI software, respectively. The estimated uncertainty of the peak frequencies is ±1 cm^{-1}.

Electron probe microanalysis (EPMA-WDS). A JEOL JXA-8530F HyperProbe electron probe microanalyzer (EPMA, JEOL USA, Inc., Peabody, MA) with a field emission gun and five wavelength dispersive spectrometers (WDS) was used to quantify the spatial distribution of rhenium in some of the glasses. The electron beam was set at an accelerating potential at 20 keV and a current of 20 nA. Metallic Re (Ted Pella, Inc., Redding, CA) was used as the standard for Re quantitative analysis. Since the baseline glass contained both Si (K_α = 1.739 keV) and Zn (K_α = 8.628 keV) with comparable X-ray energies to Re energies (M_α = 1.842 keV, L_α = 8.650 keV), special precautions were taken to prevent X-ray energy line overlap between these three elements by quantifying Re with the $M\beta^1$ peak (1.906 keV). These specific experimental conditions restricted the detection limit of Re at ≈ 336 ppm. It is due to this reason that the glass with Re concentration lower than 336 ppm was not analyzed with EPMA-WDS. Quantification utilized a ZAF data reduction routine (EPMA analysis, JEOL), which corrected and quantitated characteristic X-ray yields against mineral standards (Geller Microanalytical Laboratory, Inc., Topsfield, MA). The specific standards were: SiO_2 for Si, corundum (Al_2O_3) for Al, rutile (TiO_2) for Ti, orthoclase ($KAlSi_3O_8$) for K, albite ($NaAlSi_3O_8$) for Na, metallic Zr for Zr, MgO for Mg, ZnS for Zn, wollastonite ($CaSiO_3$) for Ca, and hematite (Fe_2O_3) for Fe. Due to the uncertainty in the absorption of characteristic oxygen X-rays in the glasses, oxygen was not measured but was calculated from cation equivalents. Randomly selected regions of the glass were measured and the compositions were averaged. Re-inclusions were observed in various regions of the glass with Re concentration of 6,415 ppm (source: Re_2O_7) and were also measured. Additionally, line scans were conducted on some of the samples in a probe mode with 256 pixels. The dwell time per pixel was set as 500 ms and pixel size was 1 μm.

X-ray absorption near edge structure (XANES) F-test data analysis. The improvement to the fit due to the inclusion each reference spectrum was determined using the F-test. Briefly, the data was fit using all four reference spectra to give the best fit. Then, the fit was repeated four times with the amplitude of one of the reference spectra set to zero each time, which produced a larger *r*-factor. For each component, $F = [(r_q^2-r_0^2)/r_0^2][(m-n)/b]$, where r_q is the *r*-factor of a fit with the amplitude of 1 component set to zero, r_0 is the *r*-factor for the fit including all components, *m* is the number of independent data (15), *n* is the number of parameters in the best fit (6), and *b* is the difference between the number of parameter in the best fit (8) and the number of parameters with one component set to zero (5). The probability that a given value of F was due to random error, p(F), was determined using Excel. If $p(F) < 0.05$, then the data supports the hypothesis that a given component is present (agreement is $> 2\sigma$), and in $p(F) < 0.01$, the data strongly supports the hypothesis ($> 3\sigma$).

Laser ablation-inductive coupled plasma-mass spectrometry (LA-ICP-MS) depth profiling. The depth profiling by time resolved LA-ICP was also carried out from the top of polished glass surface towards the bulk of glass sample as has been schematically represented in Fig. S1. Fig. S2 shows the optical microscope images of the polished glass surface from sample with Re concentration 6415 ppm (source: $KReO_4$) before (Fig. S2a) and after (Fig. S2b) laser ablation. The air bubbles present in the glass (Fig. S3) were also targeted by the laser beam in order to confirm the possible existence of rhenium in or around them. No rhenium was found, confirming their identity as air bubbles and not as trapped Re vapor. The high Re regions shown schematically in Fig. S1 are believed to be due to leaching by the potting material.

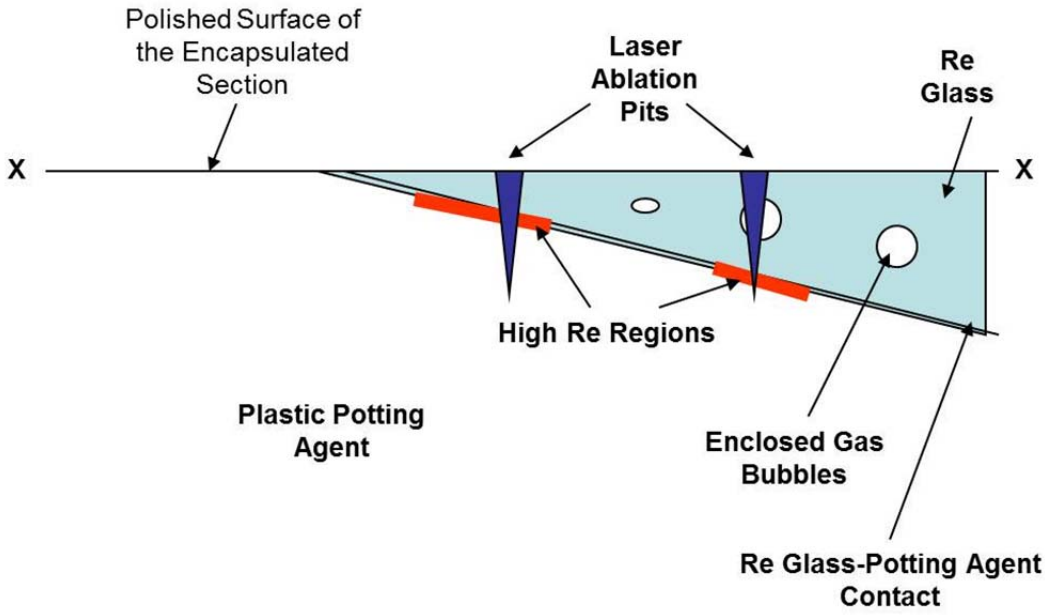

Fig. S1. Schematic of drill-down depth profiling through bubbles. Line scan from "x" to "x" corresponds to the line scan shown in photo of Fig. S2.

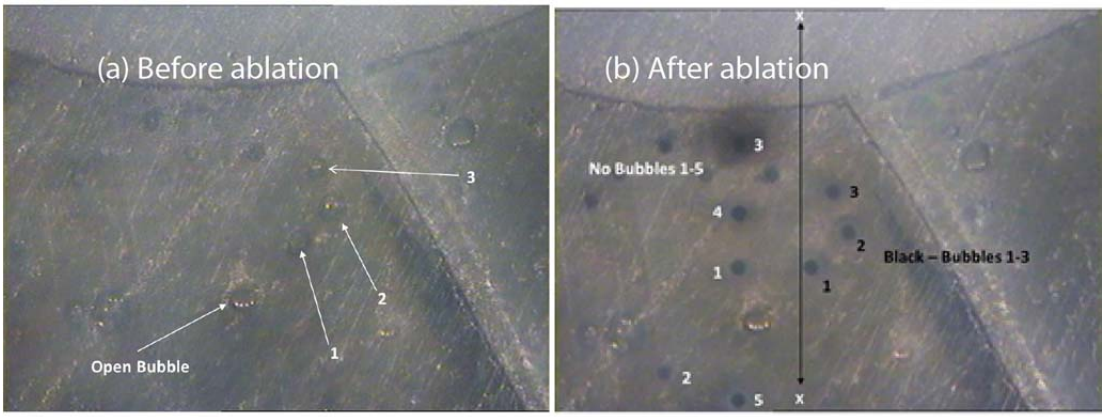

Fig. S2. Photograph of (a) before and (b) after ablations. Line scan from "x" to "x" in (b) correspond schematically to that shown in Fig. S1, even though a line scan was not done in this case. The top of the photo represents the plastic potting agent as shown in Fig. S1.

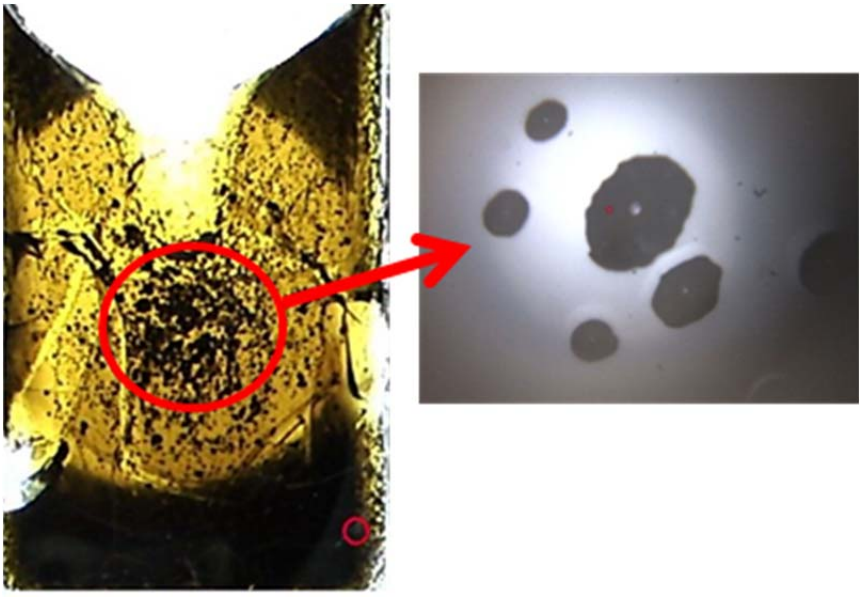

Fig. S3. Optical photograph of cross-section of 6,415 ppm (source: $KReO_4$) glass showing enlargement of air bubbles which appeared dark, whereas inclusions appeared white.

Results and discussion

Visual examination. Photographs of the glass ingot of the 6,415 ppm (source: $KReO_4$) test is shown in Fig. S2. The oblique view (Fig. S1a) shows the presence of the fused quartz ampoule surrounding the glass ingot. The top view (Fig. S1b) shows the presence of the white salt phase on top of the black glass. The cross-section with dotted lines (Fig. S1c) emphasizes the solidified funnel wherein the white liquid salt phase was contained after the glass had cooled. Similarly, the broken piece from the 6,407 ppm (source: Re_2O_7) (Fig. S2) shows the distinction between salt-covered surfaces that were on the top and those that were fractured from the bulk glass upon cooling. It is on the broken surface of this sample that the dendritic, phase-separated sulfate and perrhenate phases were found, described in the main body of this paper.

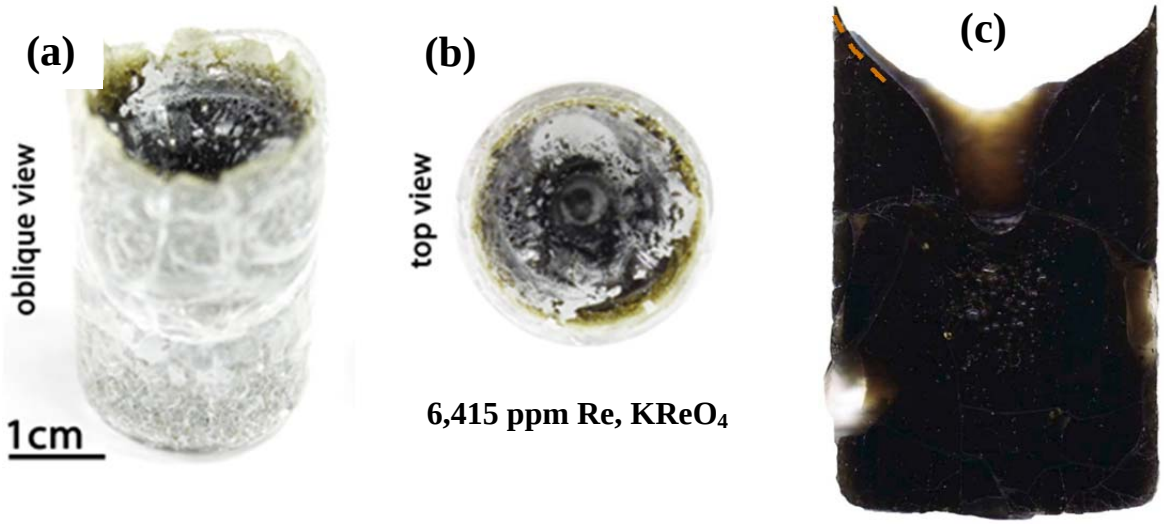

6,415 ppm Re, $KReO_4$

Fig. S1: Photographs of 6,415 ppm Re ($KReO_4$) glass test. In (c) the cross-section or shows a dotted line indicating the presence of the funnel in the cooled glass where the liquid salt phase was located.

6,407 ppm Re, Re_2O_7

Fig. S2: Photograph of 6,407 ppm Re (Re_2O_7) sample. The broken shows a dotted line indicating the presence of the funnel in the cooled glass. The top surface and fracture surfaces, both of which showed salt phases, are distinguished in the photograph.

Differential Scanning Calorimetry and the Glass Transition Temperature. The T_g was determined as the midpoint of the correspondent endothermic transition as ~530 °C and have an associated error of ±2 °C (Fig. S4). No exothermic crystallization curve could be observed until 1100 °C.

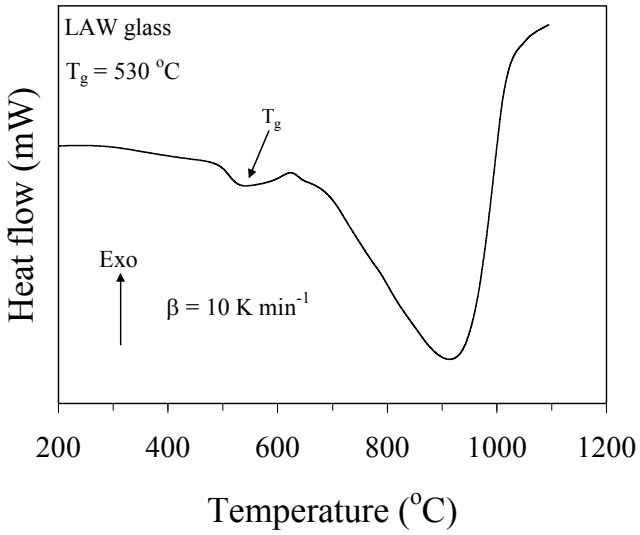

Fig. S4. DSC curve showing T_g.

Magic angle spinning nuclear magnetic resonance (MAS-NMR) spectroscopy. Fig. S5 presents the MAS-NMR spectra of the investigated glasses for ^{29}Si (Fig. S5a), ^{11}B (Fig. S5b) and ^{27}Al (Fig. S5c) nuclei. The broad ^{29}Si spectra of all the glasses imply a wide distribution of Q^n (Si) units in their glass structure. The ^{27}Al NMR spectra of the glasses manifest signal-broadening from paramagnetic-driven relaxation processes and depict the dominance of tetrahedrally-coordinated aluminum with its maxima at ~56 ppm. We could not confirm the presence of $^{[5]}$Al and $^{[6]}$Al species in these glasses with maxima at ~30 ppm and 0 ppm, respectively. (Note that the numbers in brackets before the element denote the coordination number of that species, e.g., $^{[5]}$Al is 5-coordinated Al.) In particular, the presence of five-coordinated aluminum species

cannot be neglected in these glasses as this species has been reported to exist in a variety of alkali/alkaline-earth aluminosilicate glasses.[S1] In general, in the presence of high field strength network modifiers (typically, trivalent ions), significant amounts of AlO_5 and AlO_6 polyhedra may be present in the network, even if charge balancing of all the tetrahedral units is formally possible.[S2] Similar complications of co-existing $^{[4]}$Al, $^{[5]}$Al, and $^{[6]}$Al coordination applies for (Al-B) or (Al-P) containing glasses,[S3, 4] unless Si is present and constitutes the dominating network former (as for the glasses analyzed herein). The $^{[4]}$Al resonance in all the glasses have a typical asymmetric forms with tails extending towards lower frequency resulting from the distributions in quadrupolar coupling constants.

With respect to silicon coordination in glasses, the predominant feature which determines to a first approximation the isotropic ^{29}Si chemical shifts is the number of Si and Al atoms attached to the SiO_4 unit being considered in solid aluminosilicates with increasing polymerization of Q^n building units, i.e., the shielding of central Si atom increases in the sequence $Q^0 < Q^1 < Q^2 < Q^3 < Q^4$.[S5] According to Murdoch *et al*.[S6] an increase in the number of Al next-nearest neighbors de-shields the Si nucleus, on average, by 5.5 ppm/Al neighbor. Also, the presence of several distinct modifier ions and, particularly, additional network formers result in featureless ^{29}Si MAS NMR spectra, due to the dependence of ^{29}Si chemical shift on the precise nature and spatial position of other cations and neighboring oxygen species.[S2] A more fundamental problem, however, is the presence of oxides of paramagnetic ions (Fe^{3+}, Cr^{3+}) in the studied glasses. The paramagnetic ions in excess of ≈0.5 mass% is sufficient to produce noticeably broadened NMR signals.[S7] Each one of these hurdles severely precludes the quantitative determination of speciation of the network formers in these multicomponent nuclear waste glasses. The ^{29}Si peak position for the investigated glasses lies at ~ -88 ppm. A peak

position in this range may represent highly polymerized species with many Al neighbors or less polymerized units with low or no Al neighbors. In the present scenario, the latter option with less polymerized silicate units (a mixture of Q^2 + Q^3 units) and low or no Al neighbors seem to be more feasible because of high alkali/alkaline-earth content in glasses in comparison to Al_2O_3. As mentioned above, the field strength of the modifier cation plays a key role in deciding the aluminosilicate glass structure as the extent of deviation from Al-avoidance, and thus, configurational entropy, increases with increasing cation field strength.[S8]

The ^{11}B NMR spectra of the various samples reveals two distinct NMR resonances: a primary broad peak at -19 ppm, which is typical for less symmetric planar $^{[3]}$B coordinations, and a significantly broader shoulder at -7 ppm, assigned to $^{[4]}$B coordination. It should be noted that the effect on the ^{29}Si chemical shift from boron substitutions are not well estabilished and generally depend on boron coordination.[S9] With this in mind, $^{[3]}$B are reported to produce insignificant ^{29}Si NMR peak-displacements, whereas the formation of Si-O-$^{[4]}$B motifs are predicted to give similar, albeit smaller, changes in the ^{29}Si chemical shift as those to $^{[4]}$Al (due to higher electronegativity of B compared to Al). High field ^{11}B NMR stuies are required in order to determine the $^{[3]}$B / $^{[4]}$B quantitatively. Overall, the MAS-NMR data suggest that the all the glasses have Si, Al, and some B in tetrahedral coordination, along with some B in trigonal coordination. No quantitative trends could be assessed with additions of Re up to 6,415 ppm.

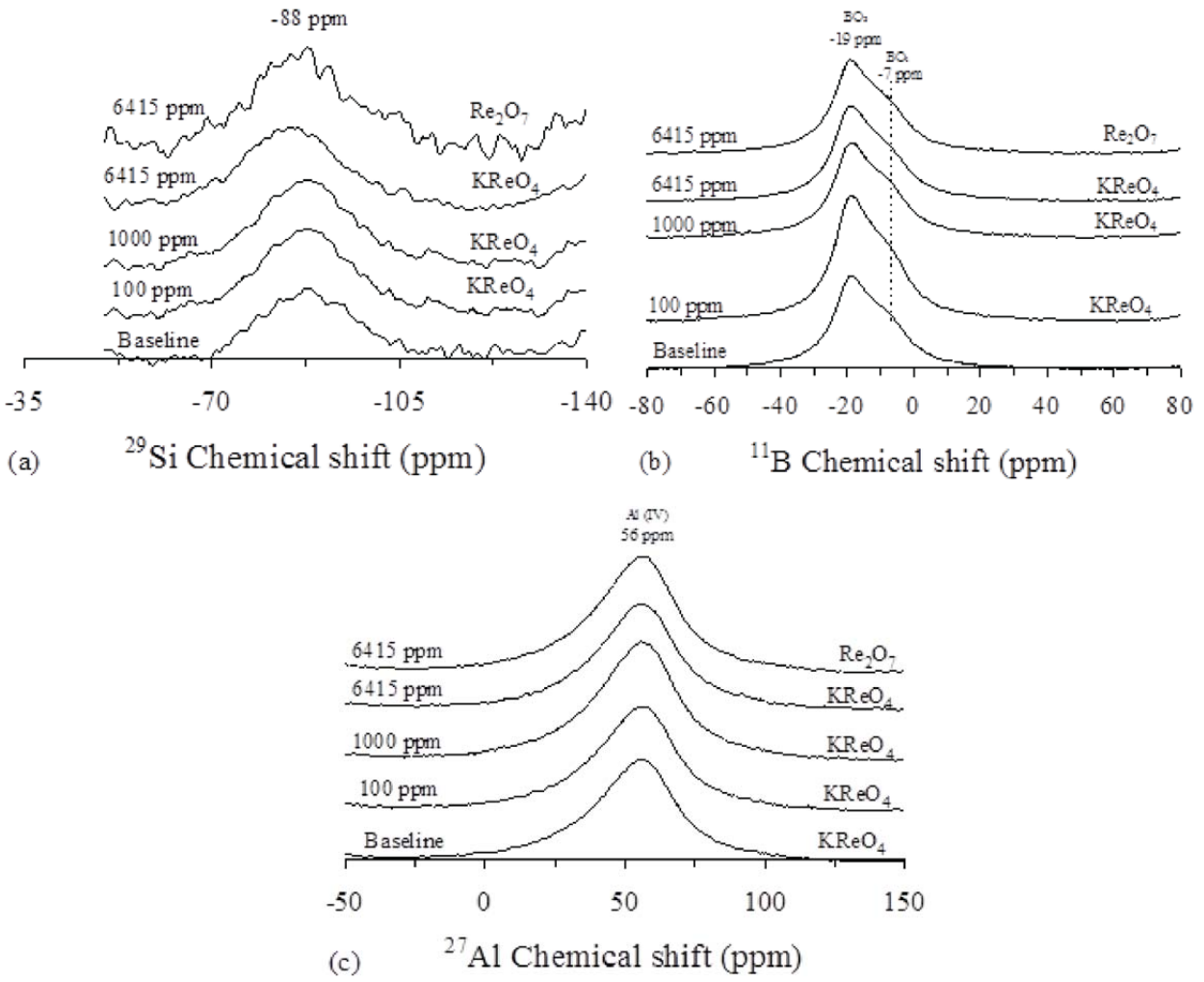

Fig. S5. MAS-NMR curves for (a) Si, (b) b, and (c) Al.

Fourier transform infrared spectroscopy. The room-temperature FTIR transmittance spectra of the investigated glasses exhibit four broad transmittance bands in the region 300–1500 cm^{-1} (Fig. S6). This lack of sharp features is indicative of the general disorder in the silicate network mainly due to a wide distribution of Q^n units occurring in these glasses, representing the degree of polymerization in the glass structure, where *n* denotes the number of bridging oxygens. The most intense transmittance bands lie in the 800–1300 cm^{-1} region, the next one between 300–600 cm^{-1} and 1300–1500 cm^{-1} regions, while the least intensive lies in the 650–800 cm^{-1} region.

The broad band in the 800–1300 cm^{-1} region is assigned to the stretching vibrations of the SiO_4 tetrahedron with different numbers of bridging oxygen atoms. In the present case, this band is centered at ~ 985 cm^{-1} suggesting a mixture of Q^2 (Si) and Q^3 (Si) units in the silicate glass network. Further, the bands in the 300–600 cm^{-1} region are due to bending vibrations of the Si–O–Si and Si–O–Al linkages while the bands in the 650–800 cm^{-1} region are related to the stretching vibrations of the Al–O bonds with Al^{3+} ions in four-fold coordination. Also, the bands at ~1420 cm^{-1} correspond to the predominant presence of boron in trigonal coordination in glasses. Since the band for boron in tetragonal coordination is overlapped by the broad silicate band in the 800–1300 cm^{-1} region; therefore, the presence of boron in tetragonal coordination cannot be neglected. We could not detect any structural changes induced by rhenium incorporation in these glasses by FTIR. Therefore, Raman spectroscopy as well as by ^{29}Si, ^{27}Al and ^{11}B MAS-NMR spectroscopy have been used to elucidate the structural changes in glasses due to their higher sensitivity in comparison to infrared spectroscopy.

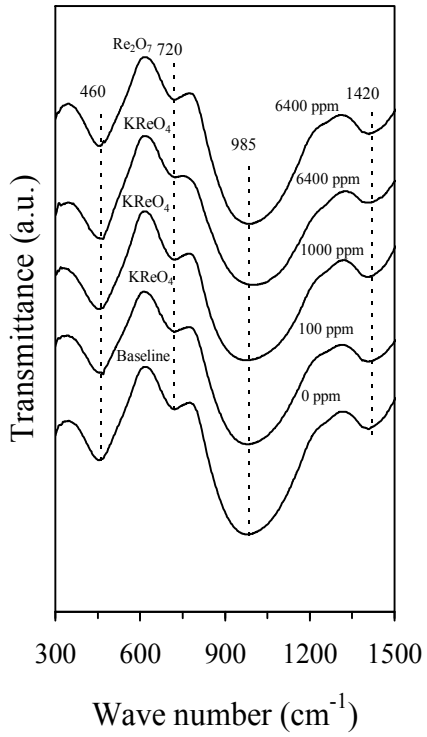

Fig. S6. FTIR transmittance spectra of selected glasses.

Raman spectroscopy. In concurrence with the XRD results, the Raman spectra of white powders on the surface of glasses with rhenium concentration: 6,415 ppm (source: $KReO_4$), 6,415 ppm (source: Re_2O_7) and 10,000 ppm (source: $KReO_4$) exhibited sharp and intense bands at ~330 cm^{-1}, ~370 cm^{-1}, 880–890 cm^{-1}, 920–925 cm^{-1} and 955–960 cm^{-1} (as shown in

Fig. **S7**a) confirming the presence of crystalline $NaReO_4$. These bands are typical for different vibrational modes of Re in the S_4 site symmetry of scheelite ($CaWO_4$) crystal structure.[S10] The band at ~960 cm^{-1} corresponds to a totally symmetric stretch, a pure bending mode at ~330 cm^{-1}, an asymmetric stretch at ~920 cm^{-1} and a combined bending and stretching mode at ~370 cm^{-1}. The band at ~885–890 cm^{-1} represents the internal mode for Re in tetragonal coordination. The remaining characteristic peaks for $NaReO_4$ which were not observed due to the spectral range of our instrument are usually centered at ~149 cm^{-1} and 181 cm^{-1} and correspond to a rotational and translational lattice mode, respectively.[S11]

All of the glass spectra exhibited broad bands in the region of 300–1500 cm^{-1} typical for borosilicate glasses (

Fig. **S7**b). No sharp or intense band could be observed in any of the investigated glasses depicting the absence of crystallinity. This observation is in contradiction with the XRD results of glasses with Re concentration 6,415 ppm (source: Re_2O_7) and 10,000 ppm (source: $KReO_4$). This discrepancy may be attributed to the heterogeneous distribution and low content of crystalline inclusions in the glass matrix. Furthermore, in addition to the typical bands for a borosilicate glass composition, a narrow but intense band was observed in all the glasses at ~ 980 cm^{-1} (

Fig. **S7**b) denoting the presence of sulfur in these glasses.

The broad band in the 800–1200 cm^{-1} region is assigned to the stretching vibrations of the SiO_4 tetrahedron with different numbers of bridging oxygen atoms. In a preliminary assessment of these glasses using FTIR spectroscopy, the absorption band is centered at ~ 985 cm^{-1} suggesting a mixture of Q^2 (tetrahedron composed of Si, Al, or B with two non-bridging oxygens, or NBO) and Q^3 (tetrahedron with one NBO) units in the silicate glass network. We could not detect any trends in structural changes induced by rhenium incorporation in these glasses by Raman spectroscopy.

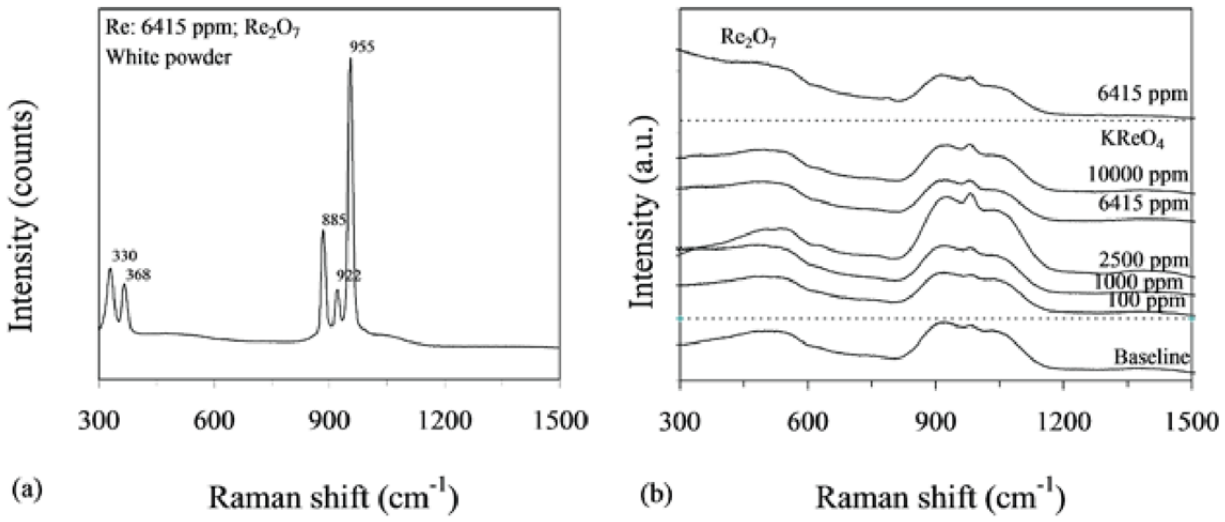

Fig. S7. Raman spectroscopy of (a) $NaReO_4$ white powdered salt, (b) selected glasses, (c) polarized spectra of baseline glass showing sulfate peak.

The Raman spectra of sulfur containing (Na, Ca)-silicate glasses has a narrow peak near 990 cm^{-1} that is similar in frequency and relative intensity to the symmetric S-O stretch mode of tetrahedral SO_4^{2-} (sulfate) ions found in aqueous solution, as well as in sodium and calcium sulfate crystals.[S12] It is noteworthy that the sulfate peak intensity in the glass spectra varies almost linearly with respect to sulfur content in the glass, where additional sulfate peaks near 460 and 620 cm^{-1}, analogous to those observed for crystalline sulfates, are found in the spectra of glasses with higher sulfur concentrations.[S13] We did not observe the additional peaks in the investigated glasses probably due to low sulfur content. According to Konijnedijk & Buster[S14] and Tsujimura *et al.*[S15] the presence of sulfur in silicate glasses does not affect the silicate glass network structure in a significant manner provided that the source of sulfur used while preparing the glass batch is an alkali sulfate salt.

In the present study, we have used Na_2SO_4 as the source for introducing sulfur in the glass batch and therefore we do not expect any significant influence of sulfur on the glass structure. Also, the possibility that sulfide species are present in the investigated glasses is low due to the high fO_2 in the quartz ampoule during glass melting (due reduction of Fe_2O_3 to FeO) but still its presence cannot be neglected.[S15] Therefore, in order to detect the presence of any other sulfur containing species in the glasses, polarized Raman spectra was acquired on the glass with Re concentration 6,415 ppm (source: Re_2O_7) as presented in

Fig. **S7**a. The HH (Horizontal transmitting, Horizontal receiving) and HV (Horizontal transmitting, Vertical receiving) polarized Raman spectra were obtained in the 300–1500 cm^{-1} range, where HH indicates that the scattered light was analyzed for an electric vector parallel to that of the incident radiation and HV indicates that the analysis of the scattered electric vector was perpendicular to that of the incident laser beam. The polarized Raman measurements demonstrate that the 972 cm^{-1} band in the spectrum of glasses arises from a totally symmetric vibration i.e., symmetric stretch of SO_4^{2-}. Since totally symmetric vibrations are strongly polarized, these bands show a marked decrease in the intensity for HV versus HH polarization conditions.

No other sulfur containing species could be detected through Raman spectroscopy. It is noteworthy that according to Mishra *et al.*[S16] in multicomponent nuclear waste borosilicate glasses, the amount of sulfur in excess of 2 mole% does not affect the glass structure while below 2 mole% it acts as network modifier. Also, the amount of alkali content in glasses has been shown to affect the sulfur solubility in LAW glass.[S17] Since, the sulfur concentration in the present study is 0.13 mole%, it acts as a network modifier.

It has been shown by McKeown *et al.*[S18] that Raman spectroscopy of borosilicate glasses can clearly see specific modes of Tc^{7+} in four-fold coordination down to concentrations of 50 ppm, but that it is completely insensitive to Tc^{4+} in six-fold coordination. However, due to the sulfate band in our samples at 980–990 cm^{-1}, the weak Raman band for Re^{7+} was not seen, as it should be about the same wavenumber as sulfate.[S19]

To test this assumption, we prepared two additional glasses without sulfur, one with and one without rhenium. The composition was chosen such that the relative molar amounts of all the components were the same as the baseline glass minus the SO_3, and the composition was renormalized. To this this "sulfate-free baseline" glass we added 6,400 ppm by weight Re in the form of $KReO_4$. We then took unpolarized and polarized (in this case VH and VV) Raman spectra on these glasses. Raman spectrometer and settings were the same as previously described except that exposure times were 100 s. The results in indicate that there is an additional polarized band due to ReO_4^- ~970 cm^{-1} that is present in the Re-containing, no-sulfate glass (

Fig. **S7**c), which is not present in the glass with no Re and no S (

Fig. **S7**b). The fact that this mode is almost exactly the same frequency as the sulfate mode explains the difficulty of using it to determine rhenium concentration in the presence of sulfate. This mode, whether sulfate or perrhenate, does not appear to be Raman active in the cross-polarized case (VH or HV).

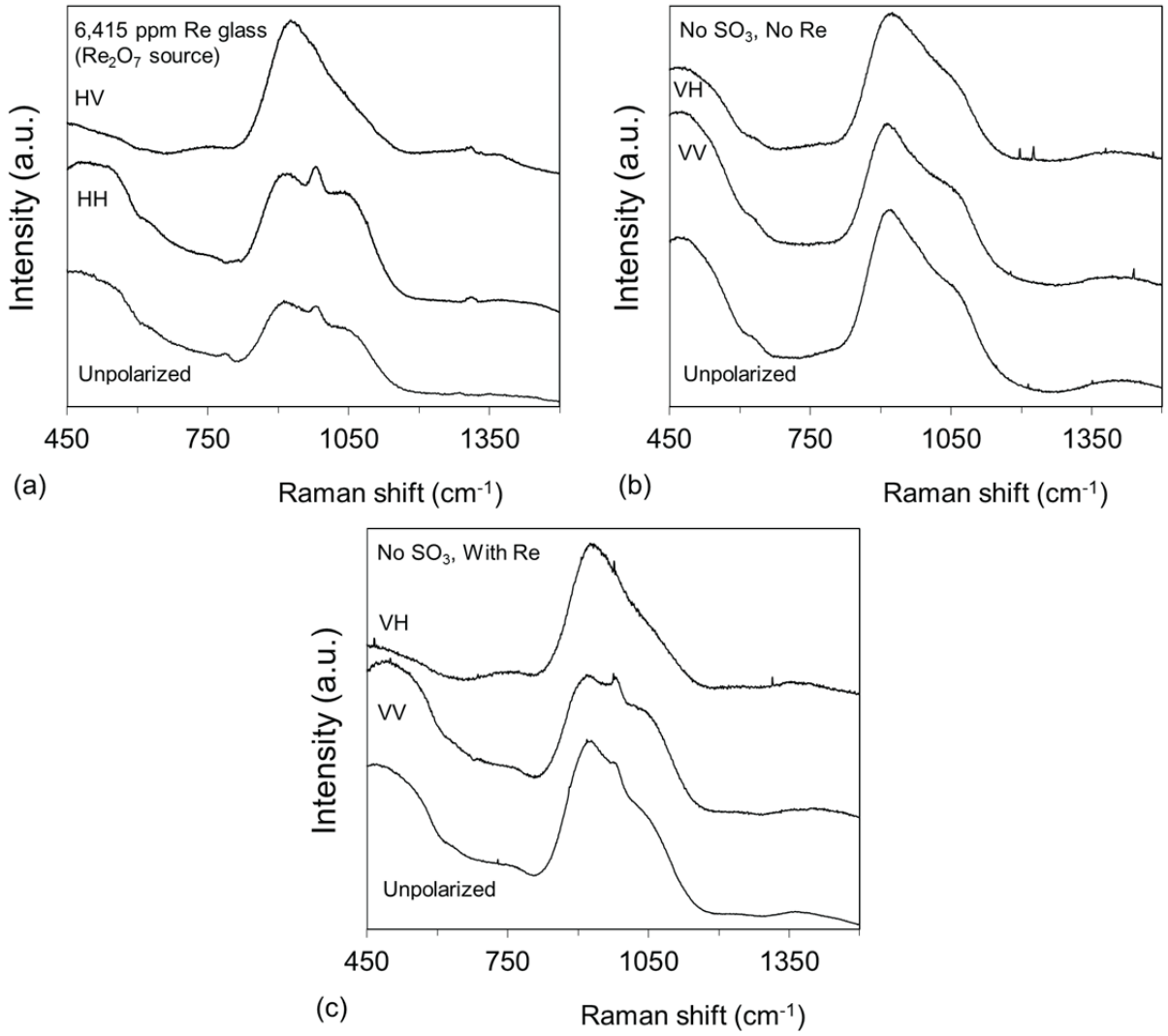

Fig. S8. Unpolarized and polarized Raman spectroscopy of (a) 6,415 ppm Re (Re_2O_7 source) glass showing peak consisting of sulphate and perrhenate, (b) glass with no sulfate and no rhenium, (c) glass with no sulfate with 6,400 ppm Re ($KReO_4$ source).

Electron probe microanalysis (EPMA-WDS). Two samples were analysed with electron probe microanalysis with wavelength dispersive spectroscopy (EPMA-WDS). Measured concentration for 6,415 ppm $KReO_4$ glass was 1,792 or 1,195 ppm Re, and for 1,000 ppm $KReO_4$ glass was 768 ppm. The quantified trend followed for variation in rhenium concentration in glasses is

similar to that observed for the data obtained from ICP-OES and LA-ICP-MS, but was lower than measured by ICP-OES. The quantitative differences in LA-ICP-MS, EPMA-WDS, and ICP-OES can be attributed to the semi-quantitative nature of the former two methods in comparison to the truly quantitative nature of the latter. The EPMA-WDS data was calibrated with Re metal. It should also be noted that ICP-OES measures total Re in the sample, both in the glass and in any crystalline rhenium-containing inclusions (such as are known to be present in samples >2,500 ppm Re), while the LA-ICP-MS and EPMA-WDS data were obtained specifically from the areas with no visible crystalline inclusions. Fig. S9 shows a line scan across the 6,415 ppm $KReO_4$ glass where a Re containing inclusion was evident. Several inclusions were found near the interface with the sample potting material, suggesting possibly that these had been dislodged or dissolved during sample preparation and re-precipitated near the potting boundary. In LA-ICP-MS similar high concentrations of Re were found at the interface between the polymer potting and the glass sample, suggesting that the polymer potting dissolved some of the Re salt.

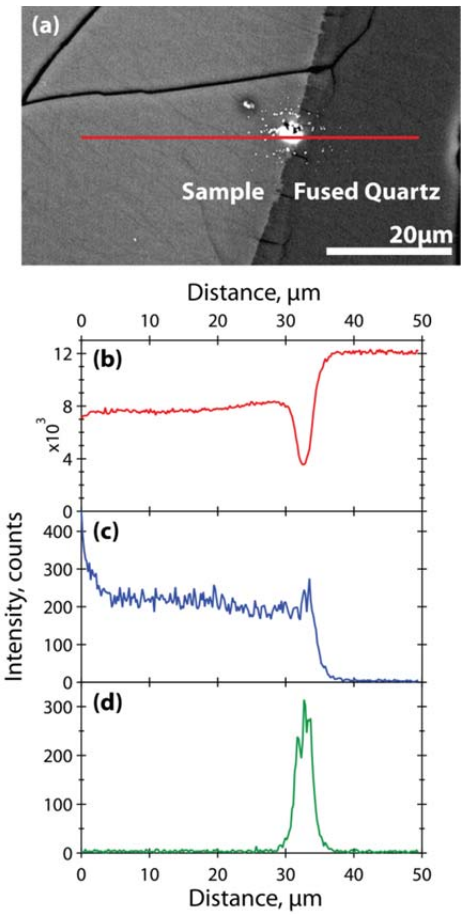

Fig. S9. WDS line scan showing (a) Re inclusion in backscattered electron as a bright spot, (b) Si counts, (c) Na counts, (d) Re counts.

Laser ablation-Inductive coupled plasma-Mass spectrometry (LA-ICP-MS) depth profiling. Fig. **S10** shows the time resolved LA-ICP data of 6,407 ppm Re (Re_2O_7 source) confirming the presence of an inclusion in the bulk of glass sample. This inclusion was visible as a white material under the surface of the glass. Similar observations were also recorded for glass with 10,000 ppm Re concentration. The experiment was conducted with a single laser spot (240 µm diameter) using 100% powder, 10 Hz rep rate, and 200 second duration.

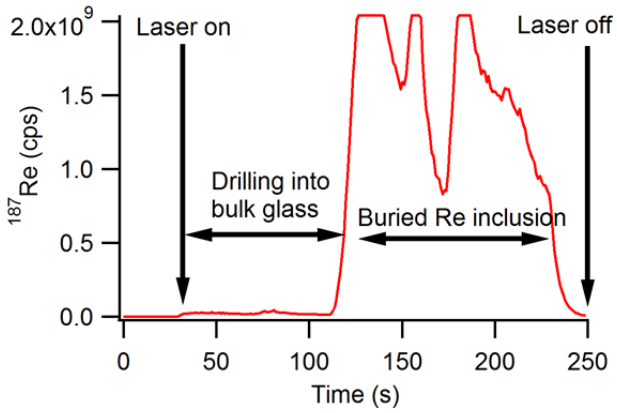

Fig. S10. Depth profiling of a white inclusion. The ^{187}Re signal saturates the detector while it is in the bulk of the inclusion, then returns to background when the whole inclusion is ablated.

References for Supporting Information

S1. K. E. Kelsey, J. R. Allwardt and J. F. Stebbins, *J. Non-Cryst. Solids*, 2008, **354**, 4644-4653.
S2. M. Edén, P. Sundberg and C. Stålhandske, *J. Non-Cryst. Solids*, 2011, **357**, 1587-1594.
S3. E. Hellmut, *Prog. Nucl. Magn. Reson. Spectrosc.*, 1992, **24**, 159-293.
S4. R. J. Kirkpatrick and R. K. Brow, *Solid State Nucl. Magn. Reson.*, 1995, **5**, 9-21.
S5. E. Engelhardt and D. Michel, *High resolution solid state NMR of the silicates and zeolites*, John Wiley & Sons, 1987.
S6. J. Murdoch, J. Stebbins, I. Carmichael and A. Pines, *Phys. Chem. Miner.*, 1988, **15**, 370-382.
S7. A. Zazzi, T. K. Hirsch, E. Leonova, A. Kaikkonen, J. Grins, H. Annersten and M. Eden, *Clays Clay Miner.*, 2006, **54**, 252-265.
S8. S. K. Lee and J. F. Stebbins, *J Non-Cryst Solids*, 2000, **270**, 260-264.
S9. L. van Wüllen, W. Müller-Warmuth, D. Papageorgiou and H. J. Pentinghaus, *J. Non-Cryst. Solids*, 1994, **171**, 53-67.
S10. S. V. Mattigod, B. Peter McGrail, D. E. McCready, L.-Q. Wang, K. E. Parker and J. S. Young, *Microporous Mesoporous Mater.*, 2006, **91**, 139-144.
S11. R. A. Johnson, M. T. Rogers and G. E. Leroi, *J. Chem. Phys.*, 1972, **56**, 789-792.
S12. R. P. Hapanowicz and S. R. A. Condrate, *J. Solid State Chem.*, 1996, **123**, 183-185.
S13. D. A. McKeown, I. S. Muller, H. Gan, I. L. Pegg and C. A. Kendziora, *J. Non-Cryst. Solids*, 2001, **288**, 191-199.
S14. W. L. Konijnendijk and J. H. J. M. Buster, *J. Non-Cryst. Solids*, 1977, **23**, 401-418.
S15. T. Tsujimura, X. Xue, M. Kanzaki and M. J. Walter, *Geochim. Cosmochim. Acta*, 2004, **68**, 5081-5101.
S16. R. K. Mishra, K. V. Sudarsan, P. Sengupta, R. K. Vatsa, A. K. Tyagi, C. P. Kaushik, D. Das and K. Raj, *J. Am. Ceram. Soc.*, 2008, **91**, 3903-3907.
S17. J. D. Vienna, P. Hrma, W. C. Buchmiller and J. S. Ricklefs, Preliminary investigations of sulfur loading in Hanford LAW glass, PNNL-14649, Pacific Northwest National Laboratory, Richland, WA, USA, 2004.
S18. D. A. McKeown, A. C. Buechele, W. W. Lukens, D. K. Shuh and I. L. Pegg, *Radiochim. Acta*, 2007, **95**, 275-280.
S19. D. A. McKeon, personal communication to J. McCloy, San Diego, CA, 2011.

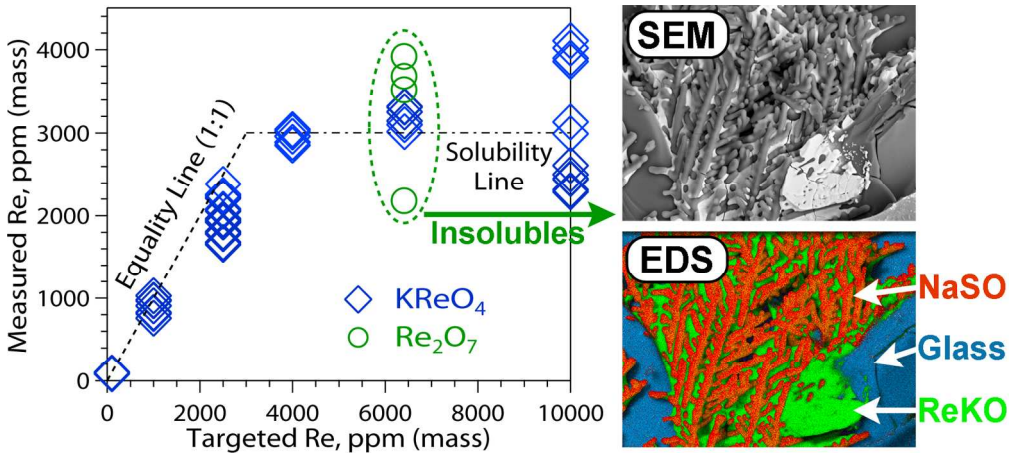
Measured Re, ppm (mass)
Targeted Re, ppm (mass)
0
1000
2000
3000
4000
0
2000
4000
6000
8000
10000
Equality Line (1:1)
Solubility Line
Insolubles
KReO4
Re2O7
SEM
EDS
NaSO
Glass
ReKO